BRANCH DETONATION OF A PULSE DETONATION ENGINE WITH FLASH VAPORIZED JP-8

THESIS

J. David Slack, First Lieutenant, USAF
AFIT/GAE/ENY/07-D04

DEPARTMENT OF THE AIR FORCE
AIR UNIVERSITY

AIR FORCE INSTITUTE OF TECHNOLOGY

Wright-Patterson Air Force Base, Ohio

The views expressed in this thesis are those of the author and do not reflect the official policy or position of the United States Air Force, Department of Defense, or the U. S. Government.

AFIT/GAE/ENY/07-D04

BRANCH DETONATION OF A PULSE DETONATION ENGINE WITH FLASH VAPORIZED JP-8

THESIS

Presented to the Faculty

Department of Aeronautical and Astronautical Engineering

Graduate School of Engineering and Management

Air Force Institute of Technology

Air University

Air Education and Training Command

In Partial Fulfillment of the Requirements for the

Degree of Master of Science in Aeronautical Engineering

J. David Slack, BS

First Lieutenant, USAF

December 2006

AFIT/GAE/ENY/07-D04

BRANCH DETONATION OF A PULSE DETONATION ENGINE
WITH FLASH VAPORIZED JP-8

J. David Slack, BS
First Lieutenant, USAF

Approved:

/Signed/	14 Dec 06
Paul I. King (Chairman)	date
/Signed/	14 Dec 06
Richard D. Branam (Member)	date
/Signed/	14 Dec 06
Mark F. Reeder (Member)	date

Abstract

Pulse Detonation Engines (PDE) operating on liquid hydrocarbon fuels are limited to operating frequencies of 35 Hz due to long ignition times from low energy ignition sources. This study shows ignition time of JP-8 can be nearly eliminated by igniting a thrust tube using a secondary detonation. A counter flow heat exchanger attached to a thrust tube utilized waste heat from the detonation process to heat JP-8 to supercritical conditions. The fuel flash vaporized upon injection into the air stream of the engine, where a detonation was produced by a spark in a 5 cm diameter, 1.37 m long tube. Part of the detonation produced in the spark ignited tube was branched through a 1.9 cm diameter crossover tube into the head of second thrust tube. A pressure transducer and hydroxyl (OH) sensor measured the combustion event that determined ignition time of the second tube was eliminated. Branch detonation was performed over a range of equivalence ratios ranging from 1.05 to 1.3. Branch ignited thrust tubes have shown a 40% improvement in deflagration to detonation transition (DDT) time and a slight improvement in DDT distance.

Acknowledgments

I would first like to thank my advisor, Dr. Paul King for the opportunity to perform research away from the computer and in an atmosphere where I could get my hands dirty. Dr. King, I appreciate your time, support, encouraging words, and guidance through this incredible learning opportunity. Thank you to my committee members, Dr. Mark Reeder and Maj. Branam for helping me refine my work.

I have to thank Dr. Fred Schauer and Dr. John Hoke for allowing a lowly thesis student to tinker around in your lab. Dr. Hoke, thank for your unending support of this research topic. I extend a special thanks to Curtis Rice for always being willing to lend a hand and teach me the practical way to accomplish a task. Even if it meant I was the one wearing the oil by the end of the day.

My research would never have been able to graduate early if it weren't for Maj. Dave Hopper and Capt. Tim Helfrich. I am forever indebted to the both of you. A special thanks to Capt. David Hoffman and Capt. Nate Terning for staying late at night and coming in on the weekend to help with testing. I can't forget Nathan Yerrick for helping me during the writing and rewriting process.

To my family, thank you for your prayers and support, you have always been a source of strength for me. Finally, to my wonderful wife, thank you for your love and encouragement that kept me going till the wee hours of the morning. After an arduous year of military separations and deployments, we will finally be able to live together in the same state! Once again, thank you to all.

Table of Contents

Page

List of Figures

Page

List of Tables

Page

List of Symbols

Acronyms

AFB – Air Force Base
AFIT – Air Force Institute of Technology
AFRL – Air Force Research Laboratory
PRTC – Propulsion Directorate, Turbine Engine Division, Combustion Science Branch
AIAA – American Institute of Aeronautics and Astronautics
CJ – Chapman-Jougeut
DDT – Deflagration to Detonation Transition
FF – Fill Fraction
FN – Flow Number
NPT – National Pipe Thread
OH – Hydroxyl
PDE – Pulse Detonation Engine
PF – Purge Fraction
PMT – Photo Multiplier Tube
PID – Proportional, Integral, Derivative
ZND – Zeldovich-Von Neumann-Doering

Symbols

A – Arrehenius constant [1/s]
A – Cross-sectional area [cm^2]
a – Speed of sound [m/s]
CI – Confidence interval
C_p – Specific heat at constant pressure [J/kg*K]
d^* - Critical diameter [cm]
E_a – Activation energy [J]
$freq$ – Frequency [Hz]
h_f° – Heat of formation [J/mol]
MW – Molecular weight [kg/kmol]
$\dot{m}$ – Mass flow rate [kg/s]
n – Number of data points
p – Pressure [Pa or atm]
q – Heat of reaction [J/kg]
R – Specific gas constant [J/(kg*K)]
R_u – Universal gas constant [J/(kmol*K)]
T – Temperature [K]
t – Time [s]
$t_{\alpha/2}$ – "T" Distribution
u – Velocity [m/s]
V – Volume [L] [m^3]
x – Experimental mean
X_i – Uncertainty variable of interest

– Number of

Greek Symbols

γ – Ratio of specific heats
λ – Cell size [mm]
σ – Standard deviation
ϕ – Equivalence ratio
ρ – Density [kg/m^3]

BRANCH DETONATION OF A PULSE DETONATION ENGINE

WITH FLASH VAPORIZED JP-8

I. Introduction

Motivation

Research on Pulsed Detonation Engines (PDE) has increased over the past ten years due to the potential for increased thermal efficiency based on constant volume combustion as opposed to a constant pressure process as in turbine engines (Eidelman et al., 1991:1). In addition, the technology is fairly low cost and is scalable for many different applications such as missile and aircraft propulsion.

Pulse Detonation Engine Cycle

A PDE is essentially a long tube closed at one end. A fuel-air mixture is injected into the tube and ignited from the closed end. The ignition will eventually cause the formation of a detonation wave by a constant volume process that produces thrust as it exits the tube. The thrust produced is proportional to the size of the tube and the frequency of the detonations. This research is focused on valved PDE cycle consisting of three phases of equal time: fill, fire, and purge.

Fill Phase

During the fill phase a fuel-air mixture is injected into the detonation tube through the fill valves as shown in Figure 1. The ratio of the volume of the fuel-air mixture to the volume of the detonation tube is called the fill fraction (FF). Once the tube is filled, the valve is closed and the fill phase is complete.

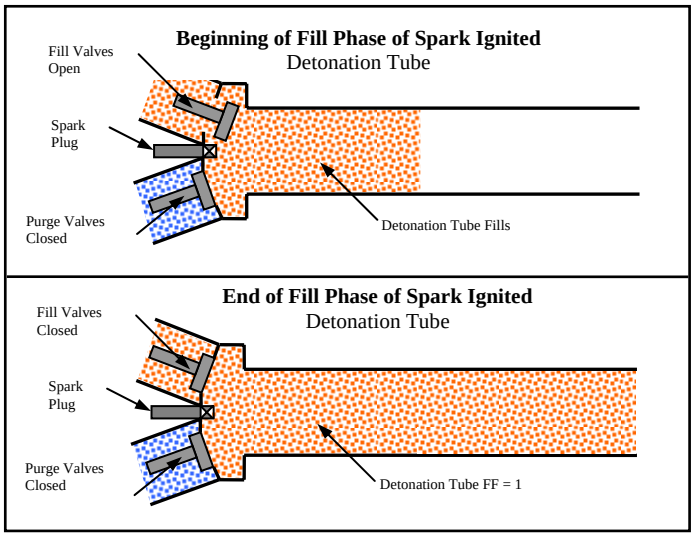

Figure 1. Schematic of the fill phase

Fire Phase

The fire phase is comprised of four different sub-phases: spark delay, ignition time, detonation to deflagration transition (DDT) time, and blow down time. The spark delay is a user specified pause between the closure of both valves and the spark initiation. The purpose is to prevent backfires during research. The ignition time is the time from the spark to the combustion of the fuel-air mixture, which for low vapor pressure fuels is approximately 7-9 msec. The DDT time is the time required for a deflagration wave formed by the ignition process to transition to a detonation wave as it travels down the tube, as seen in Figure 2, and is approximately 2-2.5 msec. The detonation wave formation process will be discussed in detail in Chapter II. Blow down is the time for the newly formed detonation wave to exit the detonation tube and is the sub-phase where thrust is produced.

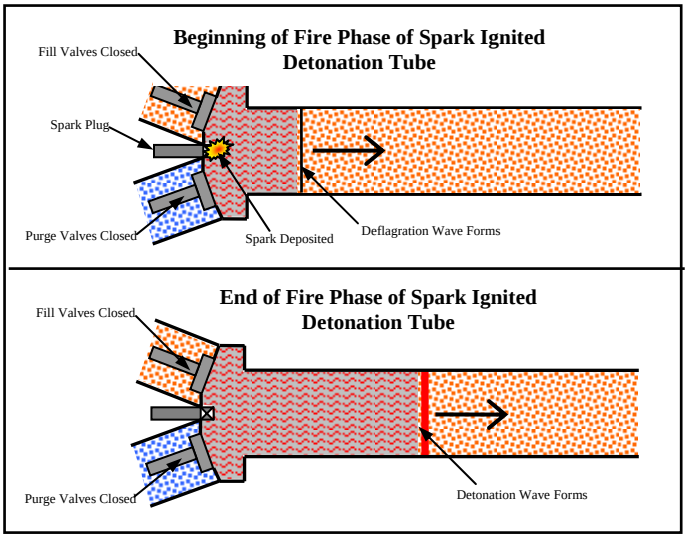

Figure 2. Schematic of the fire phase

Purge Phase

The purpose of the purge phase is to expel hot products produced in the fire phase and to cool the tube walls to prevent auto-ignition of the next cycle. The purge phase begins when the purge valve opens and air enters the detonation tube as shown in Figure 3. The ratio of purge gas volume to tube volume is known as the Purge Fraction (PF).

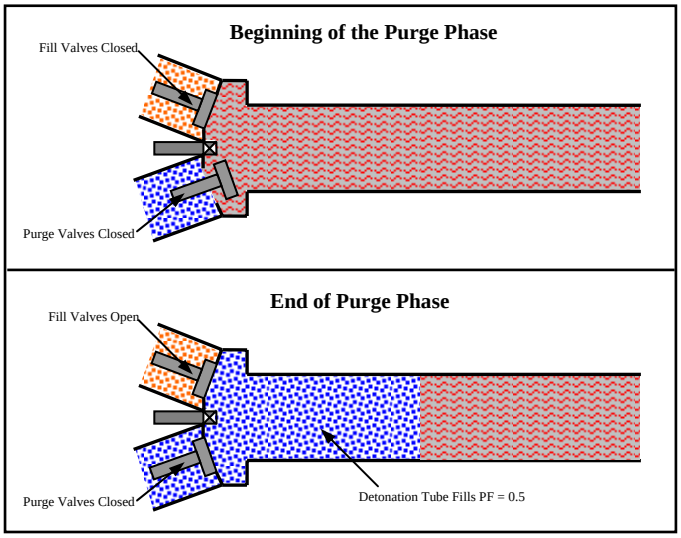

Figure 3. Schematic of purge cycle

Problem Statement

For PDEs to be a viable means of propulsion, they must be able to operate at high frequencies (Schauer et al., 2001). To obtain these higher frequencies, cycle time must be reduced. The ignition time is generally the limiting factor in PDE operating frequencies. For instance, a valved PDE using a heavy hydrocarbon fuel has an ignition time of 7 msec, a DDT time of 2 msec, and a blow down time of 0.5 msec; the total time for the fire phase would be 9.5 msec. For a system with three equal phases, the total time for one complete cycle would be 28.5 msec, corresponding to a maximum frequency of 35 Hz. Branch detonation has been shown (Tucker et al., 2003; Panzenhagen et al., 2004) to decrease ignition time and increase cycle performance in hydrogen and n-heptane. Rather than igniting the detonation with a relatively low-energy spark plug, a detonation from another source is introduced to the fuel-air mixture as seen in Figure 4.

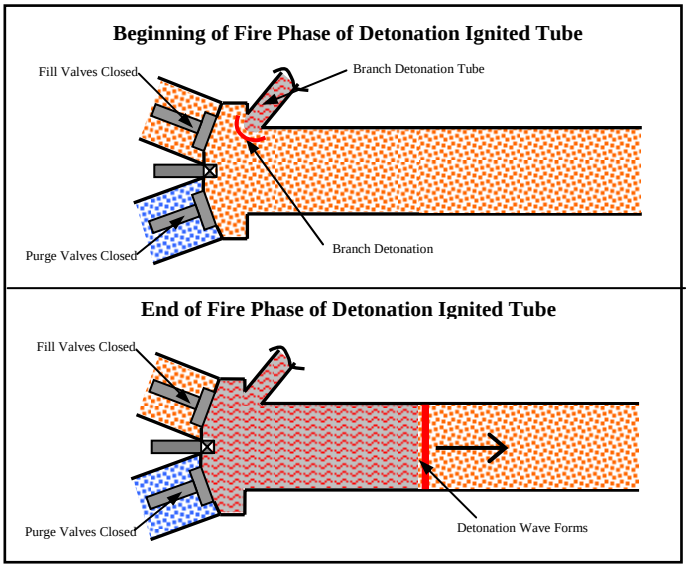

Figure 4. Schematic of branch detonation ignition

When the branch detonation wave reaches the detonation tube, the fuel-air mixture is ignited in one of two ways, strong or weak ignition.

1. Strong ignition occurs when the shock wave entering the detonation tube causes ignition and the detonation proceeds down the tube without failure. This process eliminates both ignition time and DDT time.
2. Weak ignition occurs when the energy of the combustion is insufficient to overcome expansion effects and the shock wave and combustion front separate. In this case, the reactants are ignited by the deflagration wave from the branched tube reducing the ignition time to approximately zero and decreasing the subsequent DDT time.

One goal is to create a self sustaining system where a detonation will continuously ignite each successive tube with one detonation as seen in Figure 5**.** This research is a stepping stone toward this type of design.

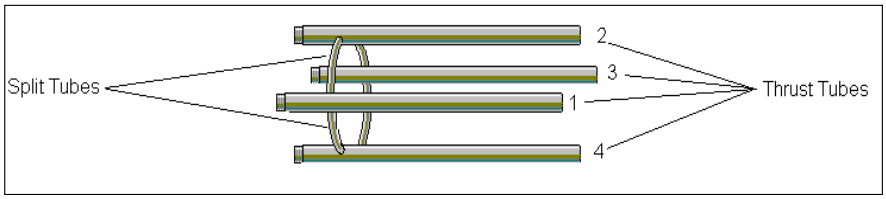

Figure 5. Concept of a Self Sustaining PDE

Recent research has shown that flash vaporized fuels decrease ignition time and reduce mixing lengths of flash vaporized fuels (Tucker, 2004; Panzenhagen, 2004). These early attempts at flash vaporization used bulky heaters that could only heat a finite amount of fuel that limited run times. Later, flash vaporization was accomplished using a counter flow heat exchanger mounted to the detonation tubes to utilize waste heat from the detonation process (Miser et al., 2005; Helfrich et al., 2006). The results of addition of the heat exchanger were the ability to run sustained steady state tests, cooling for the tube walls and a viable heating scheme that could be used on an aircraft or munitions.

JP-8 can easily detonate in a two inch tube, although this diameter would be an unacceptable diameter for a crossover tube in branch detonation. The size of the crossover tube should be of such a diameter to reduce thrust specific fuel consumption, ease the fabrication process and increase the practicality of use on future aircraft. Successful branch detonation has been demonstrated with a 19 mm (¾ in) crossover tube using hydrogen (Rolling et al., 2002). Rolling analyzed waves speeds of a detonation ignited tube with various geometries. For instance, the detonation was routed to enter the tube perpendicularly or at a 45 degree angle in an effort to cause strong ignition. In addition, wave speeds of detonations were measured through various area reductions. Rolling found branch detonation can be accomplished using a variety of configurations to cause strong ignition in a secondary tube. Work by Panzenhagen was the first to branch detonate with a flash vaporized liquid hydrocarbon fuel, n-heptane, at one equivalence ratio (Panzenhagen, 2004). She found ignition time and deflagration to detonation transition time were reduced. The following research will expound on Rolling and Panzenhagen's work by being the first to run steady state branch detonations at various equivalence ratios using waste heat from the detonation process to flash vaporize JP-8. In addition, the crossover and detonation tubes will be instrumented to create a wave speeds profile to determine type of detonations, and performance increase due to branch detonation. The following research is also the first to analyze ignition time by measuring the presence of Hydroxyl radicals.

Objectives

The objective of this research was to increase cycle performance in JP-8 by combining the proven concept of flash vaporization using heat exchangers and branch detonation. The steps follow this order:

1. Design and construct PDE tubes utilizing a heat exchanger and branch detonation geometry.
2. Detonate flash vaporized JP-8 in a 19 mm tube and measure wave speeds.
3. Ignite a detonation tube with flash vaporized JP-8 using branch detonation
4. Determine ignition time of a branch ignited tube.
5. Evaluate cycle performance by determining DDT time and location of detonation.

II. Background and Theory

The previous section briefly discussed the workings of a PDE. The following chapter discusses the theory of detonations, particularly as it applies to the current research.

Ignition Time

The first event in a PDE is ignition of the fuel-air mixture in the tube. Ignition will occur when energy added to the system is greater then the activation energy, E_a. Activation energy is energy required to start the reaction. When the activation threshold is reached, the fuel will begin to react with the oxidizer to form highly reactive radicals. As more fuel is consumed, more radicals are formed resulting in an explosion. The explosion rapidly consumes the reactants until chemical equilibrium is reached. Typical hydrocarbon fuels follow the Arrhenius Law that states the ignition time is proportional to the reaction rate. Ignition time is the time from when the energy is deposited to the system to the point of ignition. The reaction rate is directly related to the temperature and pressure as stated below (Kuo, 2005:242):

$$IgnitionTime \propto \frac{1}{RR} = \frac{1}{A} p^{-n} [\, fuel]^{-m} [oxydizer]^{-j} e^{\left(\frac{E_a}{R_u T}\right)} \tag{1}$$

where *RR* is the reaction rate, A is the Arrehnius constant, p is the pressure, [fuel] is the fuel concentration, [oxidizer] is the oxidizer concentration, R_u is the universal gas constant, E_a is the activation energy, T is the mixture temperature and n, m, and j are based on the order of the fuel in use. From Equation (1), we can see raising the temperature or pressure would decrease ignition time. Ignition time of a typical

hydrocarbon fuel would drop over 50% if the mixture was increased from 394 K to 1000 K (Helfrich, 2006:27). This drop in ignition time would still not be adequate to run at frequencies on the order of 100 Hz.

Fuel Flash Vaporization

A degradation to ignition time is the presence of fuel droplets. For example, JP-8 sprayed into air forms droplets that must evaporate to form a vapor before optimum ignition can occur. A PDE that operates at high frequencies does not allow for complete evaporation, and the presence of the droplets in the combustion region creates locally lean mixtures. Detonations are unable to form, thus hindering the performance of the engine. Past research has shown fuels can undergo a process known as flash vaporization to alleviate any presence of droplets in a fuel-air mixture (Tucker, 2005).

Liquid fuel can be heated in four different states: liquid, vapor, critical, and supercritical. All states can be characterized on a pressure-temperature diagram as shown in Figure 6. The closed curve is the vapor dome. The left line of the curve is the saturated liquid line, and the right curve is the saturated vapor line. The inner area of the vapor dome represents a region of transition from liquid to vapor given a specified temperature and pressure. The liquid region is to the left, and the vapor region is to the right of the vapor dome. The critical point is where the vapor and liquid regions meet at the top of the vapor dome. Anything above the critical point is no longer a liquid or vapor, but is now supercritical.

To flash vaporize JP-8, fuel is heated to at least 530 K with a pressure of 2 atm (Tucker 2005:94). If adequate pressure is not applied the fuel will begin to boil and

vapor will form prematurely. The fuel pressure is then rapidly and adiabatically dropped so that the fuel state is now in the vapor region as shown in Figure 6.

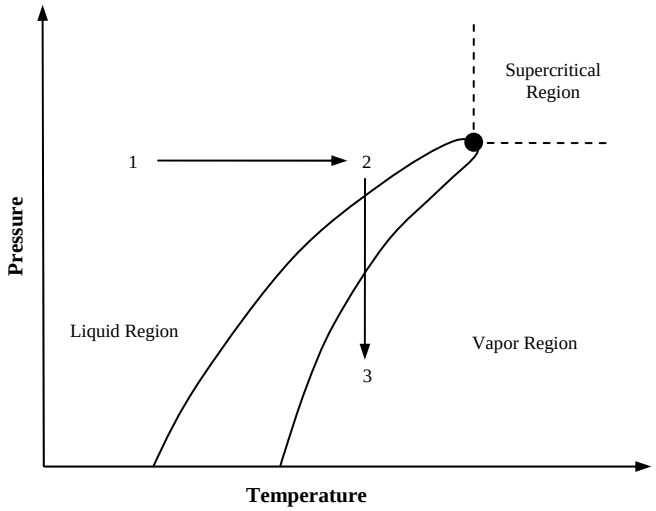

Figure 6. Temperature pressure diagram of typical hydrocarbon fuel

Detonation vs Deflagration

The ignition of a premixed fuel-air mixture produces either a deflagration or a detonation wave. A deflagration wave is a subsonic flame front sustained by heat transfer produced in chemical reactions. A detonation wave is a supersonic flame front sustained by compression waves from a trailing reaction zone. Both waves result in changes in density (ρ), pressure (p), temperature (T), and velocity (u). The downstream reactants and downstream products are viewed relative to the flame, allowing the flame front to be modeled as stationary.

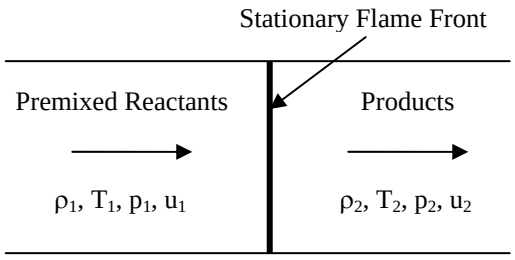

Figure 7. Diagram of stationary flame front

Deflagrations and detonations produce drastically different downstream and upstream conditions as shown in Table 1.

Table 1. Typical detonation and deflagration properties across waves (Kuo, 2005:357)

	Detonation	Deflagration
u_1/a_1	5-10	0.0001-0.03
u_2/u_1	0.4-0.7 (Deceleration)	4-6 (Acceleration)
p_2/p_1	13-55 (Compression)	≈0.98 (Slight Expansion)
T_2/T_1	8-21 (Heat Addition)	4-16 (Heat Addition)
ρ_2/ρ_1	1.7-2.6	0.006-0.25

The increase in density produced across a detonation wave will provide the momentum change to produce thrust for the PDE, whereas the deflagration properties are not conducive to producing thrust. To verify the trends stated above, one must understand the Rankine-Hugoniot relation.

Hugoniot Curve

The Hugoniot curve represents all possible downstream solutions of ρ_2 and p_2 given values of ρ_1, p_1 and heat released per unit mass, q. The basis of this relation is derived from the conservation of mass, momentum, energy and the equation of state as shown in Equations (2), (3), (4), and (5) respectively:

$$\rho_1 u_1 = \rho_2 u_2 \tag{2}$$

$$p_1 + \rho_1 u_1^2 = p_2 + \rho_2 u_2^2 \tag{3}$$

$$C_p T_1 + \frac{u_1^2}{2} + q = C_p T_2 + \frac{u_2^2}{2} \tag{4}$$

$$p_2 = \rho_2 R_2 T_2 \tag{5}$$

where p is the pressure, ρ is the density, u is the velocity, C_p is the specific heat at a constant pressure, T is the temperature, q is the heat of combustion, and R is the

universal gas constant. The equations assume one-dimensional flow, no body forces, no external heat addition, negligible species inter-diffusion effects, and no change in temperature or velocity over distance (Kuo, 2005:358). The gas is assumed to be calorically perfect, and therefore C_p is assumed to be constant. Definitions of C_p and the ratio of specific heats, γ, are used to obtain:

$$C_p = \frac{\gamma}{\gamma - 1} R \tag{6}$$

Substituting Equation (6) and (5) into Equation (4), one obtains a new expression for the conservation of energy (Kuo, 2005:360):

$$\frac{\gamma}{\gamma - 1}\left(\frac{p_2}{\rho_2} - \frac{p_1}{\rho_1}\right) - \frac{1}{2}\left(u_1^2 - u_2^2\right) = q \tag{7}$$

Combining Equation (2) and (3) yields:

$$u_1^2 = \frac{1}{\rho_1^2}\left[\frac{\left(p_2 - p_1\right)}{\left(1/\rho_1 - 1/\rho_2\right)}\right] \tag{8}$$

or

$$u_2^2 = \frac{1}{\rho_2^2}\left[\frac{\left(p_2 - p_1\right)}{\left(1/\rho_1 - 1/\rho_2\right)}\right] \tag{9}$$

Note Equation (8) is the equation of the Rayleigh line that is commonly derived without using any equation of state (Glassman, 1996:227). Combining Equations (7), (8) and (9) form Equation (10), the Hugoniot Relation (Kuo, 2005:360):

$$\frac{\gamma}{\gamma - 1}\left(\frac{p_2}{\rho_2} - \frac{p_1}{\rho_1}\right) - \frac{1}{2}\left(p_2 - p_1\right)\left(\frac{1}{\rho_1} + \frac{1}{\rho_2}\right) = q \tag{10}$$

A plot of pressure (p) to the inverse of density ($1/\rho$) given initial values p_1, $1/\rho_1$ (also known as the origin), and q, where q is the difference in the heats of formation:

$$q \equiv h_1^\circ - h_2^\circ \tag{11}$$

and

$$h^\circ = \sum_{i=1}^{N} Y_i \Delta h_{f,i}^\circ \tag{12}$$

where Y_i is the mass fraction of reactants and $\Delta h_{f,i}^\circ$ is the heat of formation of the reactants (Kuo, 2005:359). The resulting plot is the Hugoniot Curve that is all possible values of $1/\rho_2$ and p_2. The curve can be broken up into five separate regions as shown in Figure 8.

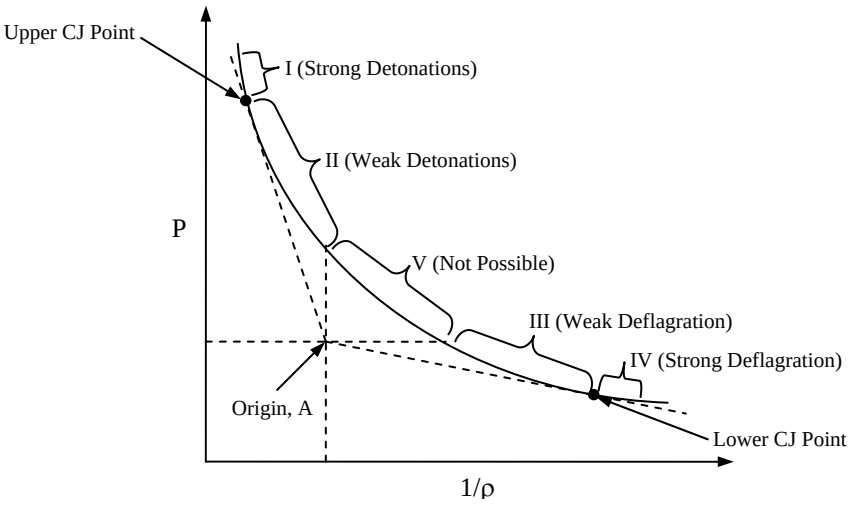

Figure 8. Hugoniot Curve broken down into sections

The Rayleigh lines drawn from the origin, (A) tangent to the curve create two points known as the upper and lower Chapman-Jouguet points, which will be referred to as CJ points for the remainder of the paper. The CJ points correspond to speeds at which detonations or deflagrations will propagate. For typical hydrocarbon fuels, the upper and lower CJ speeds are approximately 1800 m/s and 500 m/s respectively. Another naturally occurring wave structure is a choked flame which has wave speeds of approximately 1100 m/s. The other regions are created by drawing a horizontal and vertical line through

the origin. Though the curve presents all possible solutions, not all are physically feasible or possible.

To analyze the first four regions, one can examine the ratio of Δu and u_1 for compression and expansion trends. To begin, solve Equation (8) and (9) for u and take the difference to obtain Δu. Next, divide Δu by the square root of Equation (8) to obtain:

$$\frac{\Delta u}{u_1} = 1 - \frac{(1/\rho_2)}{(1/\rho_1)} \tag{13}$$

This ratio may be used to analyze the feasibility of the output solutions.

In regions I and II, $1/\rho_2 < 1/\rho_1$ which forces the right hand side of Equation (13) to be positive, meaning u_1 is greater than u_2. This concurs with mathematical and physical understanding of compression waves, thus regions I and II are feasible solutions. Further experimental analysis reveals region I is a transient state where the detonation wave temporarily travels faster than the CJ speed. This phenomenon is known as a strong detonation or overdriven wave and details will be discussed later. Region II represents weak detonations where the pressure of the products is less than that of the pressure of the upper CJ point. Weak detonations can only occur when fast chemical kinetics is present and is not relevant to the present research (Helfrich, 2005:12).

Inversely in region III, $1/\rho_2 > 1/\rho_1$ which forces the left hand side of Equation (13) to be negative. The result is u_1 is less than u_2 that means the subsonic gas is accelerated by means of an expansion wave to a higher subsonic speed (Glassman, 1996:231). The strong deflagrations of region IV require the gas velocities relative to the wave front to be accelerated from subsonic to supersonic flow. This phenomenon has never been observed experimentally, therefore region IV will be neglected (Kuo, 2005:364).

Last, region V states $p_2 > p_1$ and $1/\rho_2 > 1/\rho_1$ and according to Equation (8), the Rayleigh-line expression, u_1 would result in an imaginary number. Thus, region V is not a possible solution (Kuo, 2005:361). Analysis of the Hugoniot curve coupled with trends of expansion and compression waves reveals possible wave types seen in this report.

Another type of combustion front is a choked, or quasi-detonation wave. Choked flames is a turbulent combustion front that occurs when a rapid pressure rise will choke the flow in a cylindrical tube. The choking condition creates a sonic jet which vents the combustion front at the local speed of sound depending upon the fuel (Lee et al, 1985).

Deflagration to Detonation Transition Process

The deflagration to detonation transition (DDT) process can best be described using the tubes of the research PDE. A long tube with one closed end is filled with a vaporized fuel air mixture. A spark is deposited into the closed end of the tube and a laminar deflagration wave forms as in Figure 9.

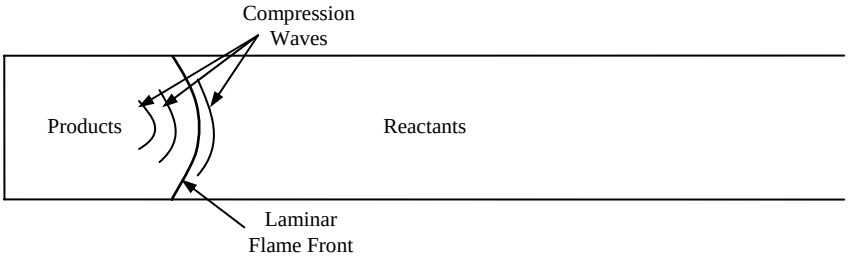

Figure 9. Deflagration wave accelerating due to compression waves

The flame front will travel at the speed of sound based on the static temperature of the reactants as in Equation (14).

$$a = \sqrt{\gamma RT} \tag{14}$$

where a is the speed of sound, γ is the ratio of specific heats, and R is the specific gas constant of the products. The combustion process increases the static temperature and the

specific volume of the products relative to the reactants. The increase in specific volume causes a compression wave to travel at the local speed of sound, which is faster than the flame front. The compression wave collides with the flame front causing the deflagration wave to accelerate. As the deflagration wave continues down the tube, product temperatures and specific volume continue to increase, forming more compression waves. Eventually the compression waves will coalesce into a shock wave ahead of the flame front (Kuo 2005:389). The shock wave induces turbulent flow of the products inducing an "explosion in an explosion" resulting in a strong spherical shock just before the formation of the detonation wave (Kuo, 2005:389) as shown in Figure 10.

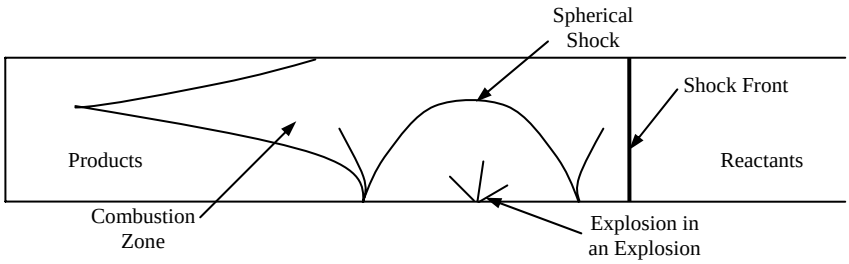

Figure 10. Explosion within an Explosion diagram

A portion of the spherical shock expands and bounces off the pipe wall forming transverse waves. Part of the spherical shock travels through the products as a sonic retonation wave. The other portion accelerates the shock front causing an overdriven detonation wave (Kuo, 2005:389) as seen in Figure 11. The overdriven wave will eventually settle to the upper CJ speed as discussed earlier.

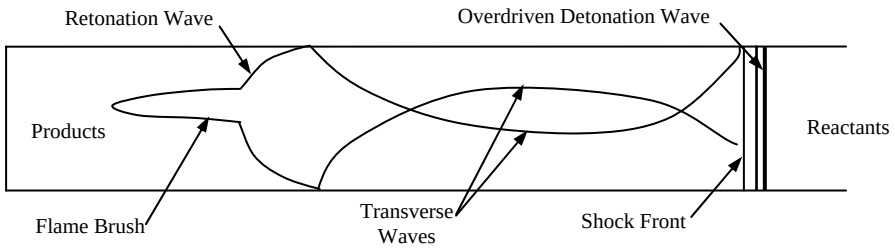

Figure 11. Overdriven detonation wave

The tube length required for DDT is not practical for use on aircraft. Therefore obstacles such as the Schelkin spiral are placed inside the detonation tubes to induce quicker DDT times and shorter DDT distances. Compression waves formed from the deflagration wave react with the spiral to form hot spots that encourage the explosions in explosions and decrease the transition distance (Tucker, 2005). In addition, wave speeds at the end of the spiral tend to be overdriven.

The 1-D Zel'dovich-Von Neumann-Döring Model

The previous sections have described the differences of deflagration and detonation waves, including how a detonation wave is formed. The next step is to understand how a detonation wave is sustained. Zel'dovich, Von Neumann, and Döring independently developed a one dimensional model of a detonation wave known as the Zel'dovich-Von Neumann-Döring (ZND) model (Kuo, 2005:381). The ZND model has become the classic example of detonation propagation. They postulated a detonation wave can be modeled in three zones: shock wave, induction, and reaction zones. Figure 12 is a graph of variations of physical properties through each of the three zones.

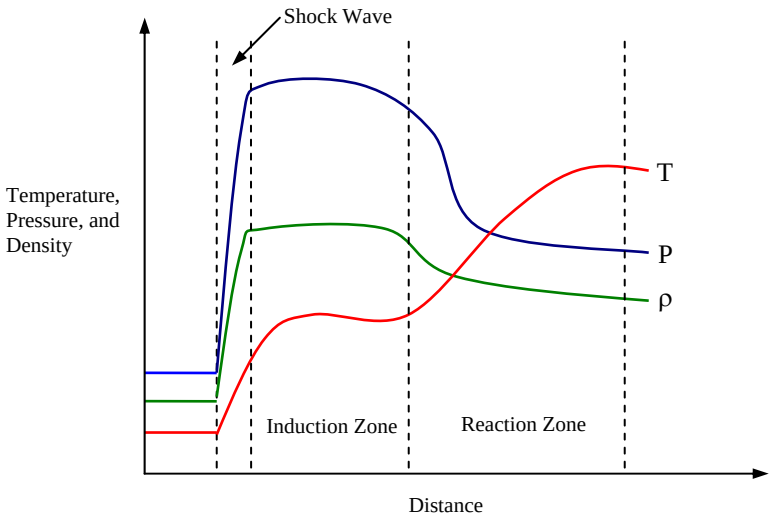

Figure 12. Generic diagram of property variations in the ZND model (not to scale)

The shock is on the order of a few mean free paths thick and is assumed as a jump discontinuity. Pressure, temperature and density are substantially increased by the shock waves and allow for quick reaction rates required to sustain a detonation wave. Without the effects of the shock wave, a detonation wave would fail. The region behind the shock wave, known as the induction zone, contains negligible variation in gas properties. The reaction zone produces a large increase in specific volume that creates the compression waves to sustain the detonation front.

Detonation Structure

The structure of a detonation wave provides insight to wave propagation and provides a basis for design requirements. There are two types of detonation structures, multi-head and single-head spin. Multi-head detonation structures are modeled in a long narrow channel and assumed to be governed by two dimensional effects. Detonation structure can be observed by propagating a detonation wave along a soot-coated film in a channel. A fish scale pattern is deposited on the smoke film (Kuo, 2005:384). Figure 13 represents the structure found on the smoke foils.

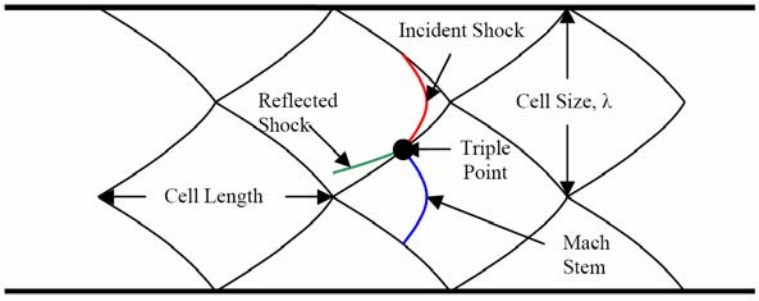

Figure 13. Two dimensional drawing of detonation cell structure

The detonation front is composed of alternating shock waves called the Mach stem and incident shock. The waves propagate by energy released in the combustion of the fuel-air mixture in the channel. The collision of all three waves, Mach stem, incident shock, and

reflected wave, produces a shear discontinuity called the triple point. As the detonation travels down the channel the triple point erases the soot on the foil to create the fish scale pattern, also known as the triple point track (Glassman, 1996:255). The closed shapes of the detonation structure as shown in Figure 13 are called cells. The transverse spacing is the cell size and the longitudinal spacing is the cell length. Cell size is the basis for many important design choices found later in this report.

Single-head spin detonations occur in smooth circular tubes and are the lowest possible stable mode of detonation (Kuo, 2005:403). They are formed by an increase in transverse wave strength that increases the three dimensional effects. These effects together form a single shock front with a trailing flame front that rotates about the tube axis. The wave front travels at the CJ speed but a measured axial velocity would be lower due to the tangential velocity component (Kuo, 2005:403). A typical wave front path is shown in Figure 14

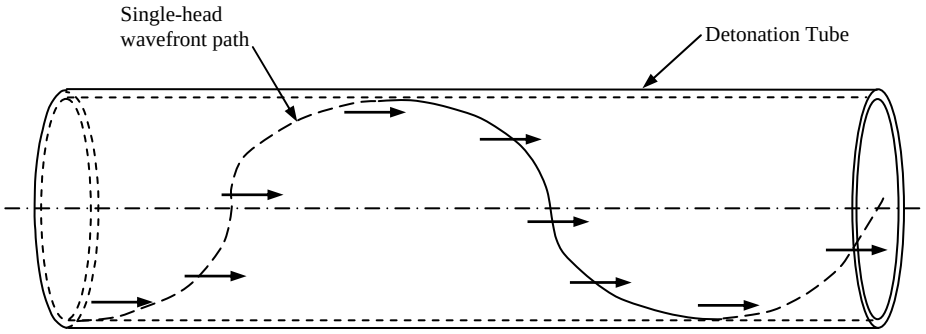

Figure 14. Path of a single-head detonation wave in a tube

The onset of a single head spin detonation at a specific fuel concentration and at the minimum tube diameter can experience a phenomenon known as galloping. When a single head spin detonation encounters an obstacle, it can lose and then almost instantaneously regain its wave structure. Galloping can cause velocity fluctuations in excess of 10% of the CJ speed (Kuo, 2005:410).

Critical Diameter

The branch detonation tube does not produce thrust, and should be constructed from a minimum diameter to reduce specific fuel consumption. The minimum tube diameter, also known as the critical diameter, of a single-head spin detonation proposed by Kogarko and Zel'dovich and verified by Lee (Kuo, 2005:406) is the relation between cell size and circumference:

$$\lambda = \pi d^* \tag{16}$$

where λ is the cell size and d^* is the critical diameter (Kuo, 2005:406). Equation (16) sets the design requirement for a multi-head detonation to transition and propagate as a single-head spin detonation down a smaller diameter tube.

Cell Size Sensitivity

Cell size is sensitive to many conditions such as fuel properties, nitrogen dilution, fuel-air ratio and wave speed. The cell size of various low vapor pressure hydrocarbon fuels has been experimentally determined and categorized according to the energy required by a combustion system to initiate a direct detonation, also known as the direct initiation detonation energy. A typical low vapor pressure hydrocarbon fuel combusted in a stoichiometric fuel air mixture requires approximately 1MJ of energy to directly initiate a detonation (Tucker, 2005:25). The relationship between cell size and direct initiation detonation energy is given by the expression:

$$E_{DID} = 3.375\lambda^3 \tag{17}$$

where E_{DID} is the direct initiation detonation energy and λ is the cell size. Typically, the heavier the molecular weight of the fuel the larger the cell size as shown in Figure 15.

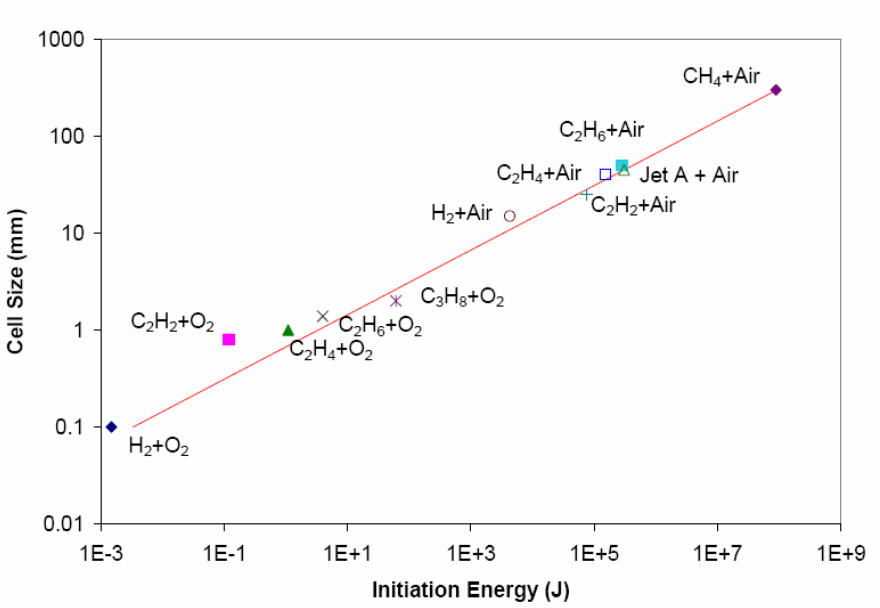

Figure 15. Graph of Cell Size v Initiation Energy

Figure 15 also points out an effect known as nitrogen dilution that causes an exponential increase in the cell size and initiation energy. One can see in Figure 15 that hydrogen combustion in air has a larger cell size than combustion in pure oxygen and therefore, requires more energy. Coupled with the idea of direct initiation energy and nitrogen dilution is equivalence ratio. Equivalence ratio is defined as the ratio of the actual fuel air ratio to that of the stoichiometric fuel air ratio as defined by Equation (18):

$$\Phi = \frac{\left(\frac{\dot{m}_{fuel}}{\dot{m}_{air}}\right)_{actual}}{\left(\frac{\dot{m}_{fuel}}{\dot{m}_{air}}\right)_{st}} \tag{18}$$

where Φ is the equivalence ratio, $\dot{m}_{fuel}$ is the actual fuel mass flow rate, $\dot{m}_{air}$ is the actual air mass flow rate, and $\left(\frac{\dot{m}_{fuel}}{\dot{m}_{air}}\right)_{st}$ is the stoichiometric ratio of fuel and air mass flow rate.

If Φ <1, the fuel-air mixture has an excess of air, and the excess nitrogen from the air will increase cell size. The equivalence ratio can be decreased until no combustion can take

place; this is the lean limit. If $\Phi > 1$, then there is not enough air to fully combust the fuel. The remaining unburned fuel is unused or wasted energy. A large amount of excess fuel can quench the combustion process completely; this is the rich limit. Figure 16 shows the relation of equivalence ratio to cell size of various hydrocarbons.

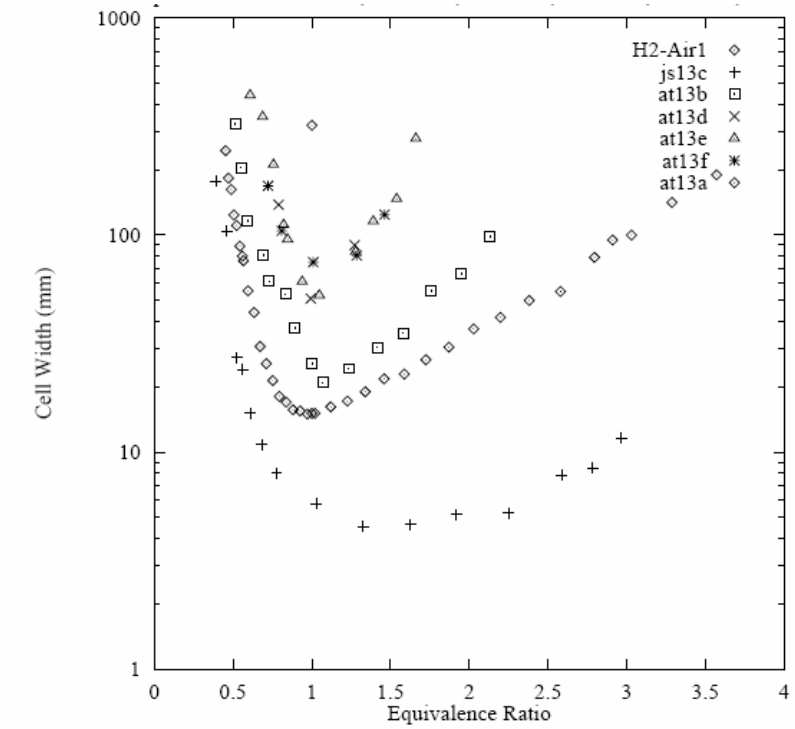

Figure 16. Cell size versus equivalence ratio of various hydrocarbon fuels used with permission (Kaneshige et al, 1997)

One observation from Figure 16,is it is better have a rich mixture. The lean side of the curve is much steeper and increases the cell size more quickly than the rich side. The other observation is that the optimum equivalence ratio is around 1.1. At a macroscopic level and equivalence ratio of 1.0 will appear to be ideal for liquid fuels, but the microscopic level there can be areas of localized lean conditions due to fuel droplets.

Detonation cell size decreases with overdrive of the wave, which is defined as the ratio of the velocity of the overdriven detonation to the velocity of the corresponding CJ detonation wave (Saretto, 2005). Overdriven waves were to a degree of 1.4 showed a

decrease in cell size to approximately one tenth of the CJ velocity cell size. The decrease in cell size is temporary and will increase as the wave decays to the upper CJ speed, this process usually occurs within 10-15 widths of the combustion channel (Saretto, 2005).

Detonation Diffraction

Branch detonation uses a detonation from one tube to ignite a second tube. The detonation exiting the crossover tube experiences a process known as diffraction. Understanding of this process is vital to determine the ignition time of a tube ignited by a detonation. Diffraction is the process of expansion from a planar detonation to a detonation with a spherical geometry. This phenomenon is experienced during abrupt changes in area (Schultz, 2000:37) such as a detonation exiting a crossover tube. As a planar detonation wave emerges, strong expansion fans at the tube walls reduce the energy of the shock front. If the energy released from the combustion front is greater than the energy lost due to expansion effects, the detonation will not fail. If the expansion effects dominate, the shock wave will decouple from the combustion front and the detonation will transition to a spherical deflagration wave (Schultz, 2000:39). Degrees of diffraction are categorized as: super-critical, near-critical and sub-critical cases (Schultz, 2000:5). Schultz uses hydrogen detonation waves propagated through a 25mm (0.98 in) diameter tube into a 152mm (6 in) square test section. The test section was fitted with transparent portions to record shadowgraphs of diffraction in each of the three regimes.

Super-critical

The super-critical case describes the successful transition of a detonation wave into an unconfined region. Empirical data indicates for a detonation to survive the diffraction process in a circular tube, the detonation size must be at least thirteen times the cell size, 13λ (Kuo, 2005:404). A combustion front that is 13λ produces enough energy to overcome expansion losses of a detonation wave entering an unconfined space. The shadowgraph in Figure 17 shows the evolution of a super critical detonation wave. Note that the shock wave does not detach from the combustion front, and the detonation wave survives the expansion process.

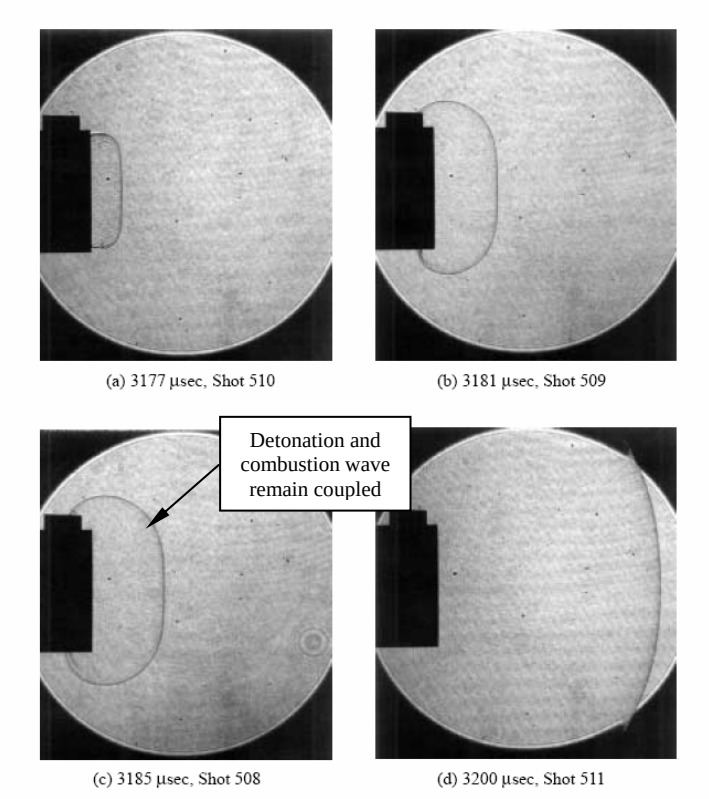

Figure 17. Shadowgraphs of super-critical detonation diffraction of hydrogen and oxygen mixture used with permission (Schultz, 2000:114)

Near-critical

Near critical diffractions result in a partial failure as the shock wave decouples from the combustion front closest to the edges of the tube. The detachment of the shock wave can be seen in the comparison of Figure 18(a) and Figure 18(b). Surviving portions of the detonation front produce localized explosions. The result is a highly non-uniform front that explodes outward to re-initiate the detonation front (Schultz, 2000:116).

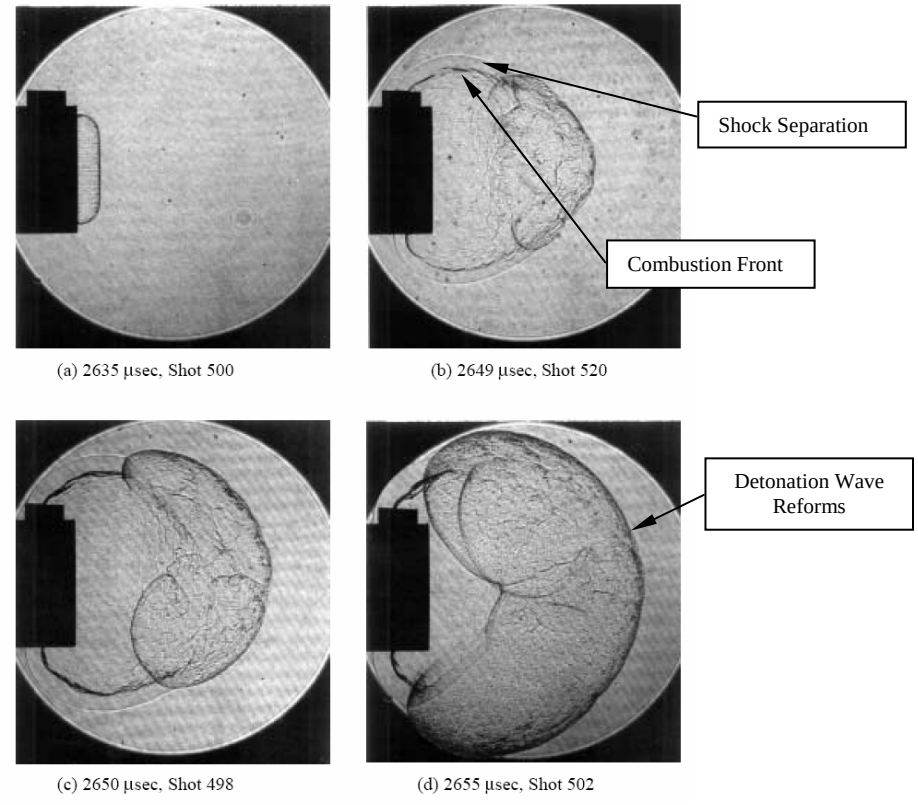

Figure 18. Shadowgraphs of near-critical detonation diffraction of hydrogen and oxygen mixture used with permission (Schultz, 2000:119)

Sub-Critical

The final regime, sub-critical, is a complete failure of the detonation wave. The sudden expansion causes the shock wave to decouple from the combustion front as seen in Figure 19c. The result is a spherical deflagration wave as seen in Figure 20d.

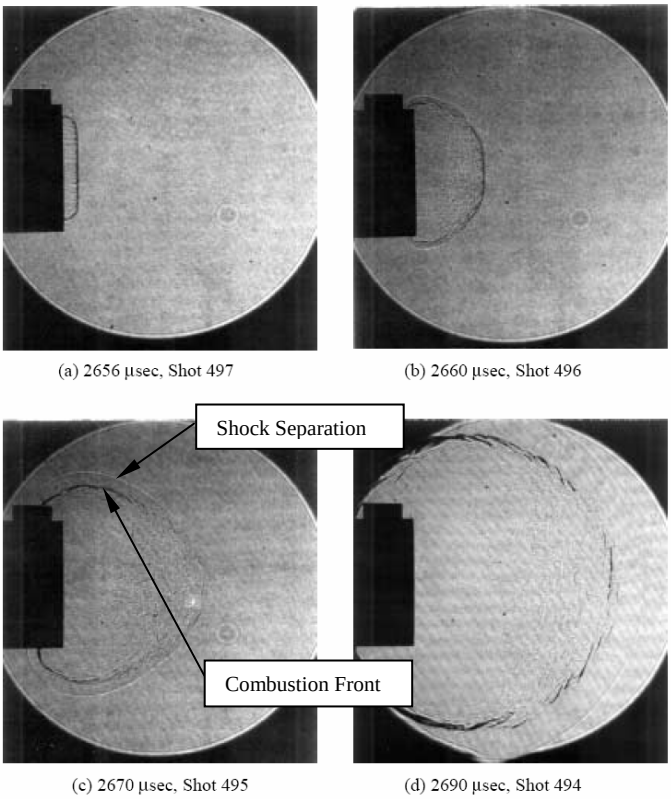

Figure 19. Shadowgraphs of sub-critical detonation diffraction of hydrogen and oxygen mixture used with permission (Schultz, 2000:117)

For all cases, the shadowgraphs indicate ignition is of the hydrogen-air mixture in the open area is instantaneous. If the entering detonation is super or near-critical, the fuel is ignited by the shockwave coupled to the combustion front. If the entering detonation is sub-critical, the fuel-air mixture is ignited by the combustion front of the deflagration wave.

Chapter Summary

Ignition of a fuel-air mixture produces a deflagration wave, which through the aid of a spiral, can quickly transition to a detonation wave producing thrust as it exits a detonation tube. The structure of a detonation wave can exist in two forms, multi-head and single spin. Multi-head detonation waves are characterized by cells that are the result of a shear discontinuity caused by the intersection of three different shock waves. The diameter of a tube that a single head spin detonation can propagate is dependent upon the cell size. The cell size depends on the properties of the fuel, nitrogen dilution, and equivalence ratio. A detonation wave expanding into an unconfined space is categorized into three different regimes. To successfully transition a detonation without failure the wave diffraction must be super-critical or near-critical. In all cases, ignition of the fuel-air mixture in the unconfined space is instantaneous.

III. Materials and Methodology

D-Bay Facility

The current PDE research was performed at Wright Patterson Air Force Base, Ohio, Building 71A, D-Bay. The PDE program is managed and sponsored by the Air Force Research Laboratory, Propulsion Directorate, Turbine Engine Division, Combustion Sciences Branch (AFRL/PRTC) in conjunction with the Innovative Scientific Solutions, Inc. (ISSI) contractor.

The PDE facility is a 21,200 m^3 (748,670 ft^3) explosion proof test cell originally intended for turbojet testing. The facility contains a 267,000 N (60,024 lb_f) turbojet thrust stand and an exhaust tunnel was retrofitted to support the PDE (Schauer, 2001). The facility also contains workspace and tools to perform engine maintenance and minor part fabrication. The fuel and control rooms are separated from each other and the test cell by two foot thick, steel reinforced, concrete walls. Most liquid fuels are contained, stored and prepped in the fuel room. The control room is used for engine control, data collection and real time monitoring through closed circuit cameras. The engine is operated from a dedicated computer using a virtual LabVIEW generated control panel. High speed wave data is collected on a separate computer also using an in house program created in LabVIEW. The fuel room and engine operation can be monitored and recorded from the control room cell through a closed circuit television.

Air Supply System

The air for the fill and purge cycles is compressed by an Ingersoll-Rand Pac Air Compressor (Model# PA 300V) capable of producing 40 m^3/min (1412 ft^3/min) rated to 6.8 atm (100 psi) and stored in a 4.5m^3 (159 ft^3) receiver tank (Serial# 10894, Buckeye

Fabrication Co.). Due to size and noise levels, the compressor and receiver tank are stored in a separate room in D-Bay known as the compressor room. The air is routed out of the compressor room into the test cell under the test stand where it is split into main and purge air. Calibrated critical flow nozzles are installed inline with the air lines and provide a known mass flow rate for a given upstream pressure. The upstream pressure is measured by a pressure transducer located upstream of the flow nozzles in the main and purge lines. The temperature of the air lines is measured with T-type thermocouples also located upstream of the flow nozzles. The pressures and temperatures are assumed to be stagnation values. Components of the air supply system are seen in Figure 20.

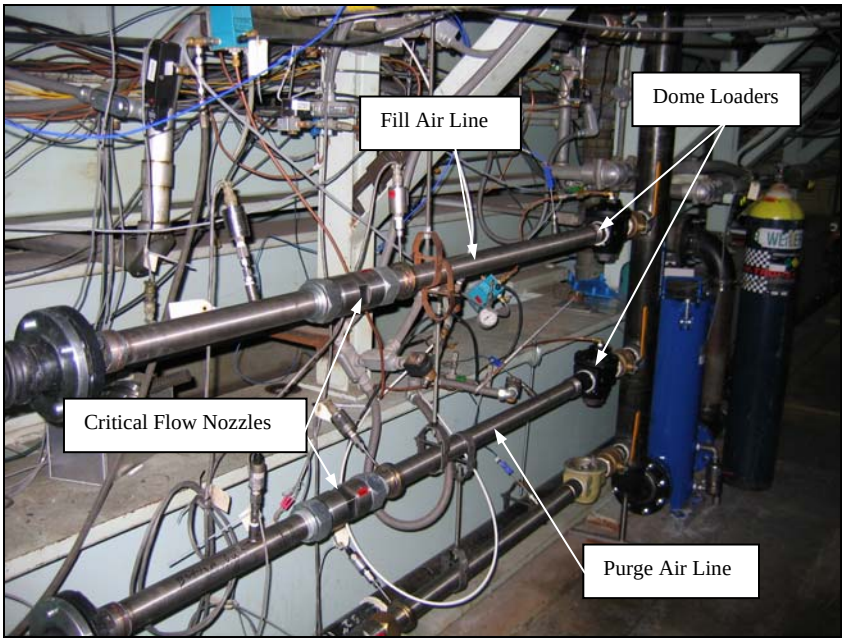

Figure 20. Main and purge air lines

The upstream main and purge temperature and pressures are monitored in the control room. The LabVIEW program calculates the required air mass flow rate using Equation (19):

$$\dot{m} = \frac{(\#_{tubes})(freq)(V_{tube})(FF)(P)}{RT} \tag{19}$$

Where $\#_{tubes}$ is the number of tubes used in the experimental setup, freq is the frequency of the motor, V_{tube} is the tube volume, FF is the fill fraction, P is the pressure of the air, R is the specific gas constant for air and T is the air temperature of upstream air. All the variables are either entered or measured by LabVIEW. Tescom Electropneumatic PID controllers (Model# ER 1200) actuate dome loaders powered by high pressure nitrogen bottles to obtain the desired pressure differential. Surge tanks are located downstream of each orifice place to attenuate any effects of compression waves. The fill air is then routed to a Chromalox Circulation Heater (P/N 053-500870-187). Amperage is entered into LabVIEW which is then translated to an upper temperature limit to the Chromalox temperature controller (Model# 2104). The air is then sent to the main air fill manifold where it is mixed with fuel.

Deoxygenating System

Only liquid JP-8 fuel was used in this research. Past studies (Panzenhagen, 2004; Tucker, 2005; Helfrich, 2005) have shown that JP-8 contains dissolved molecules of oxygen that react with the fuel at temperatures above 450K to form particulates in a process called coking. The use of flash vaporization in this research requires a process known as sparging to dislodge oxygen molecules from the fuel. Fuel is placed in a 61L (16 gallon) stainless steel fuel reservoir and sealed. The bottom of the reservoir contains a hollow coil with holes drilled in it as seen in Figure 21.

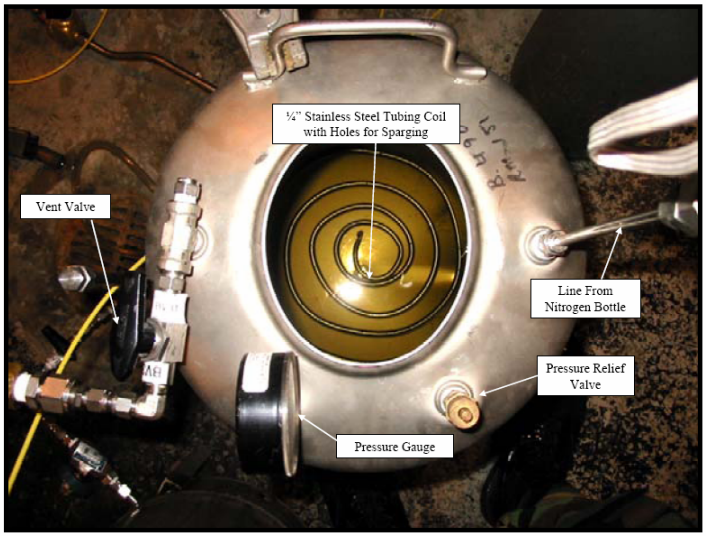

Figure 21. Top view of sparging reservoir

Nitrogen flows through the coil and bubbles up through the fuel agitating and dislodging the dissolved oxygen molecules from the fuel. The flow rate of the nitrogen is increased by hand until bubbles could be audibly heard through the sealed reservoir. The nitrogen and freed oxygen molecules are vented out the top of the reservoir to the atmosphere. A detailed description of the sparging process is given by Tucker (Tucker, 2005:61-66).

Liquid Fuel Supply System

Upon completion of the sparging process the fuel is moved into the fuel accumulators. The accumulators are pressure vessels with a concentric bladder containing fuel. Nitrogen gas is injected between the bladder and accumulator wall and squeezes the bladder, moving the fuel through the system. The D-Bay fuel system uses two 9.46 L (2.5 gallon) Greer hydraulic accumulators rated to 204.14 atm (3,000 psi). High pressure nitrogen from two bottles is regulated by a dome loader controlled by a Tescom Electropneumatic PID Controller (Model# 26-2015T24A272). The Tescom is controlled by the user in the control room, which will be discussed later. The components of the fuel room are shown in Figure 22.

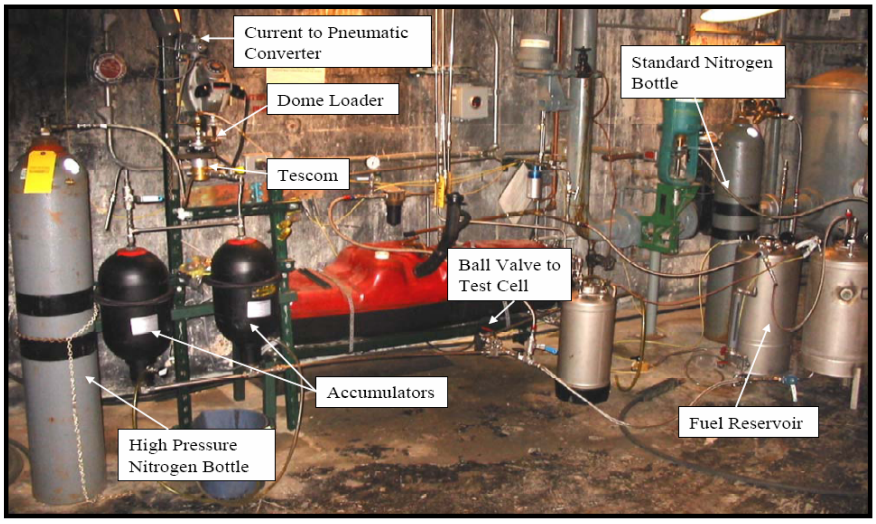

Figure 22. Liquid Fuel System in the D-Bay Fuel Room

To fill the accumulators, fuel lines to the engine are closed, and the valves connecting the reservoir to the accumulators are opened. The fuel reservoir is pressurized by a standard nitrogen bottle and pushes the fuel into the accumulators. Once the reservoir is depleted, the valves from the reservoir are closed, and the fuel line is opened as in Figure 23.

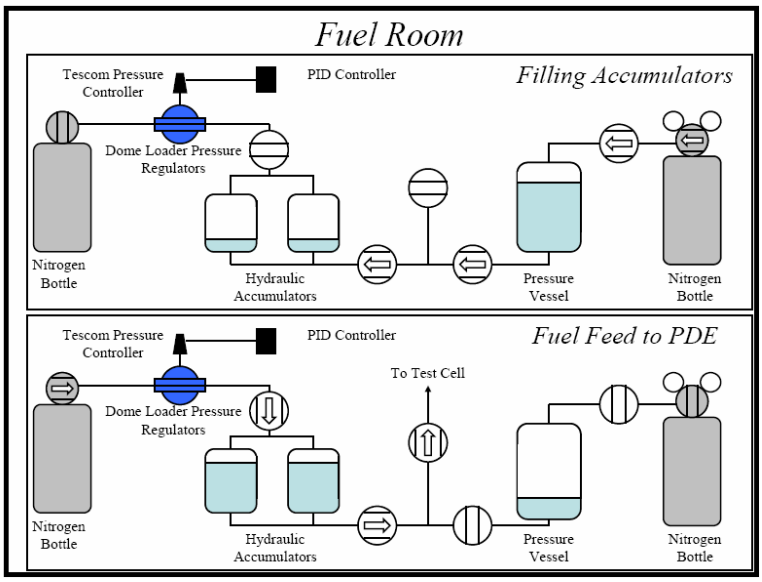

Figure 23. Schematic of liquid fuel system

Fuel flow is measured by a Flow Technology Turbine volumetric flow meter (Model# FT4-8AEU2-LEAT5) and a thermocouple located downstream of the flow meter. The

outputs are used to calculate equivalence ratio and fuel density. When filling the fuel line, the flow meter is bypassed to prevent damage by over spinning the turbine. The fuel then flows through a pneumatic valve known as the last chance valve. The last chance valve is a safety mechanism tied to emergency switches throughout D-Bay. If any safety switches are triggered, fuel flow is stopped. After passing the last chance valve, the fuel then enters the test stand and is heated to supercritical conditions by a counter flow heat exchanger. Finally the fuel is mixed with the air using Delevan flow nozzles. Two permanently mounted spray bars containing the flow nozzles, shown in Figure 24, are placed perpendicular to the flow in the air manifold.

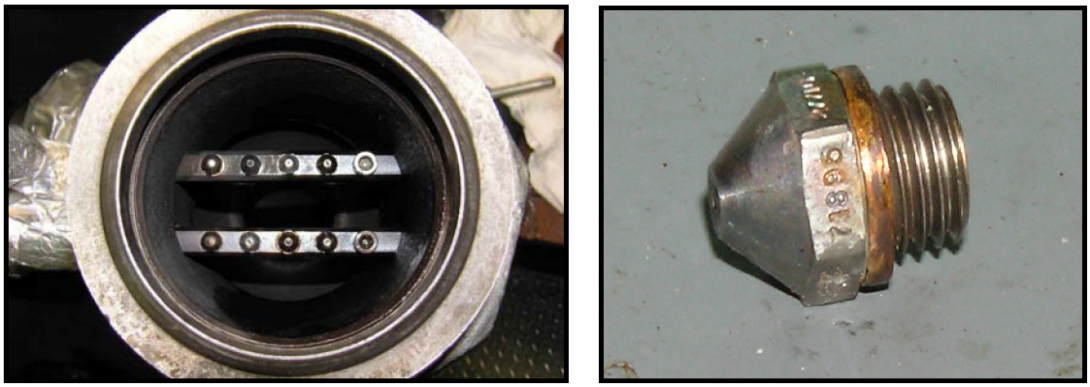

Figure 24. Manifold spray bar (Left) and Delevan flow nozzle (Right)

Each nozzle has a calibrated flow number that can be combined with other nozzles to achieve larger values. The required flow number to achieve a desired mass flow rate is determined by Equation 20:

$$FN = \frac{\dot{m}_{fuel}}{\sqrt{p_{fuel}}} \sqrt{\frac{\rho_{cal}}{\rho_{fuel}}} \tag{20}$$

where $\dot{m}_{fuel}$ is the mass flow rate of fuel as determined from the equivalence ratio in Equation 17, p_{fuel} is the pressure of the fuel, ρ_{cal} is the calibrated density of fuel, and ρ_{fuel} is density of fuel exiting the heat exchanger which are determined from temperature and

pressure readings in the fuel line. The PDE was configured to provide a constant mass flow rate and equivalence ratio due to the flash vaporization method. Details are discussed by Helfrich (Helfrich, 2006:50).

Engine

The research engine in D-Bay uses a General Motors Quad 4 engine head with dual overhead camshafts. Four intake/exhaust valves control the amount of fuel-air mixture into the engine. Up to four thrust tubes can be mounted in line with the engine head openings, numbered 1-4 in Figure 25.

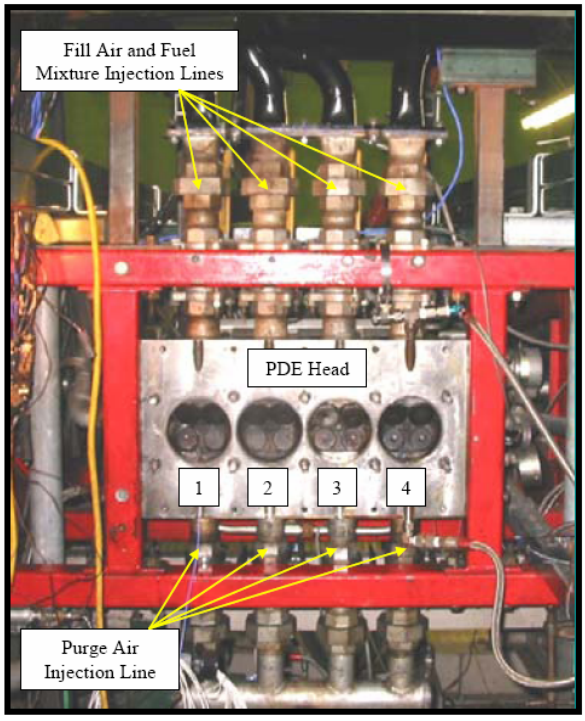

Figure 25. Photograph of GM Quad 4 engine head with thrust tubes labeled

The valves are controlled by the camshafts that are in turn driven by a variable speed Baldor Electrical motor (Model# M4102T). Within each combustion chamber are two intake and two exhaust valves. The intake valves provide fill and the exhaust valves provide purge air. Valve timing will be discussed later. The fill manifold is located

above the head, and the purge manifold is located below the head. Each cylinder is connected to the manifold by a ball valve. The valves physically opened or closed during the setup, which allows engine runs to use any combination of openings 1-4. The intake manifold is covered with insulation, not shown in Figure 25, to reduce heat loss of the vaporized fuel.

Engine cooling is performed by running water from a 1.5 hp Teel electric water pump (Model# 9HN01) through the existing water cooling ports in the engine head. Automotive oil is pumped from a reservoir by a Viking electric oil pump (Model# FH432) to the valve train to provide lubrication and additional cooling.

Ignition System

The ignition system is controlled by the LabVIEW program in the control room. A BEI optical encoder (Model# H25) measures the position of the camshaft and sends it to the control room. The computer then translates that information to valve position. When both valves are closed, the program sends a signal to a 12 VDC MSD Digital DIS-4 ignition system to provide four sparks of 105-115 mJ each. The user can specify a spark delay to decrease chance of backfires. The PDE uses modified NGK automotive spark plugs. The spark plugs have the grounding electrode removed and a small piece of tube welded to the end.

Heat Exchanger

The heat exchanger is constructed of two 15 in long concentric tubes. The inner tube is 2 in stainless schedule 10 pipe, and the outer tube is 2.5 in schedule 10 pipe. Square stainless steel endplates are welded to each side to enclose the annular region of the heat exchanger. Two ¼ in Swagelock unions are welded at opposite ends as fuel

ports and are radially offset 180 degrees as seen in Figure 26. Fuel enters the heat exchanger from the lower port and exits the through the top to take advantage of natural convection to circulate the fuel through the heat exchanger. The heat exchanger is rated for pressures at 5.516 MPa and 588 K. More information on the design of the heat exchanger is found in research performed by Miser (Miser, 2005:49-50).

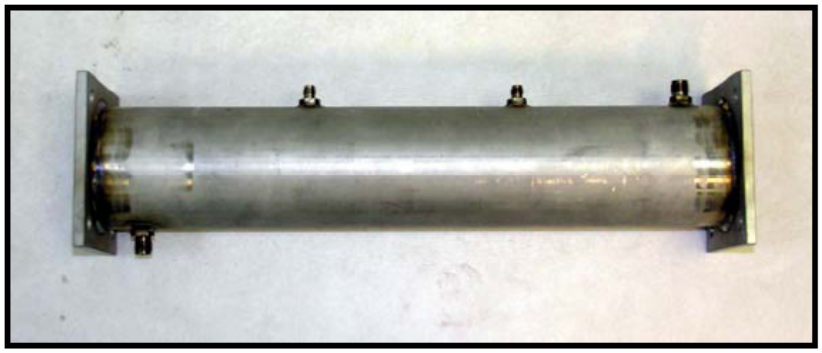

Figure 26. Photograph of 15 inch heat exchanger

Detonation Tubes

Each test consisted of two detonation tubes mounted to positions 4 and 2 on the engine head. The detonation tubes will be referred to by their corresponding head locations. Position 4 and 2 were used for timing purposes discussed later. Tube 4 is a spark ignited detonation tube and its purpose is to produce repeatable and consistent detonations. In addition, tube 4 heats the fuel in the heat exchanger for flash vaporization. Tube 2 is the detonation ignited tube. A crossover tube allows a detonation to branch from the spark ignited tube to the head of the detonation ignited tube. The pipe used for tube 4 and 2 is 51 mm (2 inch) diameter which is near the smallest diameter to achieve a multi-head detonation in JP-8/air. Likewise, a 19 mm (¾ inch) diameter was chosen for the crossover tube to match the minimum diameter criterion of a single-head spin detonation as shown in Equation (17). In each case, readily available materials were selected. English units will be presented for the remainder of chapter III.

Spark Ignited Tube

Tube 4 consists of four major components: steel tubing, a heat exchanger, a mounting plate, and a spiral. The pipe components are all stock 2 in schedule 40 steel pipes threaded with male 2 inch national pipe thread (NPT) and connected together by female 2 in pipe collars. Special mounting brackets were fabricated to connect the heat exchanger endplates to the NPT steel tubes. The endplate was constructed from quarter inch type 316 stainless steel, and the tubing was 2 inch schedule 40 NPT pipe. A gasket was placed between the heat exchanger and each mounting bracket to prevent leakage. A ¾ inch hole was drilled in the wall of a standard 2 inch steel schedule 40 pipe nipple, and a male ¾ inch Swagelock fitting was then welded to the hole to connect the crossover tube. The pipe nipple was attached using female pipe collars. Ion probe ports are located on each side of the fitting to determine wave speeds across the branch detonation port. Tube 4 is 53.5 in long with the heat exchanger located between 17 and 35 inches measured from the head. The heat exchanger was originally positioned closer to the head, but the location did not supply sufficient heat for flash vaporization. All the thrust tubes are threaded onto a 0.5 inch stainless steel mounting plate machined to attach to existing stock engine head bolts. A Schelkin-type spiral extends down the first 3 ft of the detonation tube. The branch detonation nipple was positioned at the end of the spiral to take advantage of smaller cell size resulting from overdriven detonation waves.

Crossover Tube

The crossover tube is ¾ inch stainless steel, 0.065 inch wall thickness tube with Swagelock fittings on each end. The tube is approximately 48 inches in length and is

fitted with ion probe ports throughout to measure wave speeds. This is the same crossover tube used in similar research by Panzenhagen (Panzenhagen, 2004).

Detonation Ignited Tube

Tube 2 is 55 inches in length and is constructed from pieces of 2 inch schedule 40 steel pipe that are connected by steel 2 inch steel female collars. Tube 2 is threaded into a special mounting plate. A ¾ inch tube was welded to the mounting plate and fitted with a Swagelock fitting for the crossover tube to connect as seen in Figure 27. The purpose is to directly port the detonation into the head of tube 2 to cause ignition.

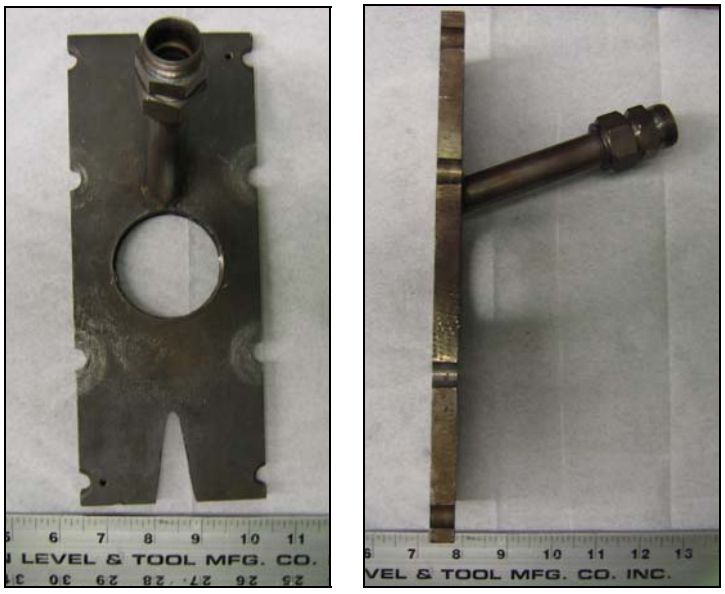

Figure 27. Photograph of front and side view of tube 3 mounting plate

Tube 2 was also fitted with a 3 ft Schelkin-type spiral. Past research with JP-8 has shown a minimum of three foot spiral is needed to produce repeatable detonations in a spark ignited detonation (Helfrich, 2005). A stock engine head gasket was used to create a seal between the engine block and the detonation tube mounting plates. A picture of the setup is shown in Figure 28 and a schematic of the setup is in Figure 29.

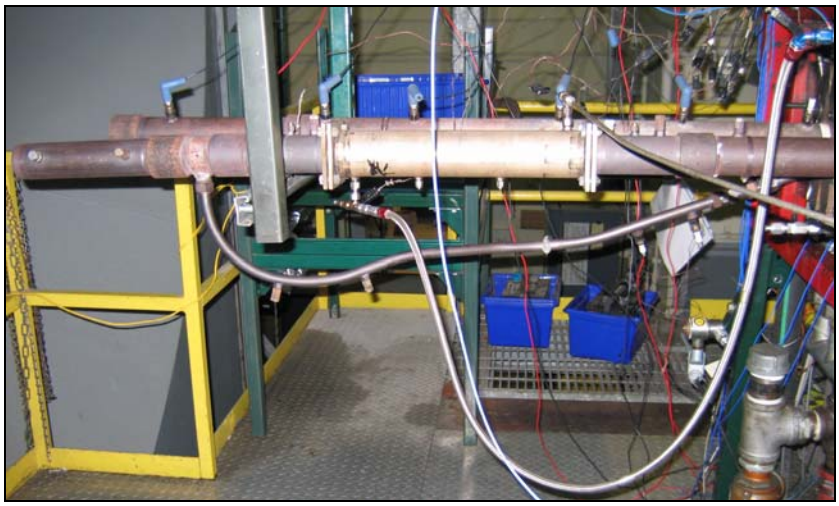

Figure 28. Photograph of branch detonation setup using head locations 4 and 3

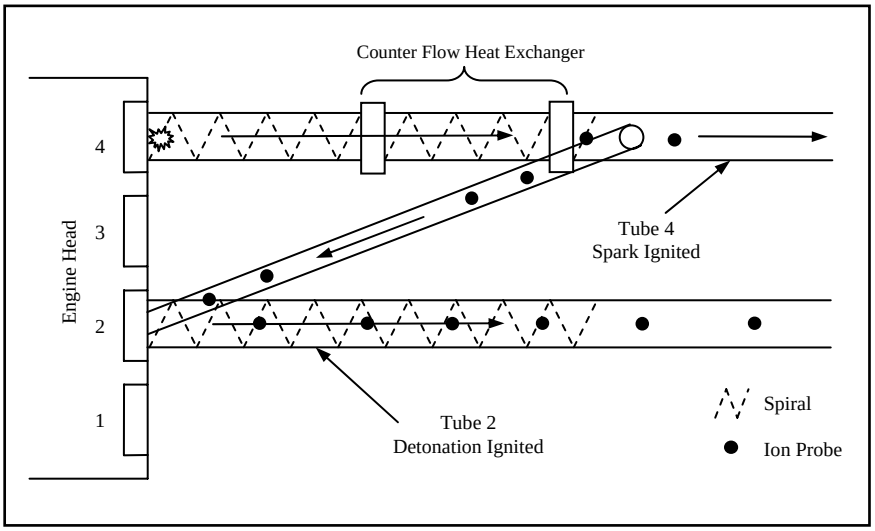

Figure 29. Schematic of branch detonation

Engine Timing

The firing order of the tube locations based on the camshaft is 1-3-4-2 and each tube location is 90^{o} offset from each other. For the detonation to reach the head of the tube 2 during the fire phase, a calculation determined the operating frequency of the engine to be 20 Hz. This frequency allows 16.667 msec for each phase of the cycle each successive tube location lags by 12.5 msec. The breakdown of cycle times at 20 Hz for tube 4 and 2 is shown in Table 2.

Table 2. Phase times relative to tube 4

	Time [msec]	
Phase	**Tube 4**	**Tube 2**
Fill	0 - 16.7	12.5 - 29.2
Fire	16.7 - 33.4	29.2 - 45.9
Purge	33.4 - 50	45.9 - 62.5

The time from a spark in tube 4 to a detonation wave reaching the head of tube 2 is approximately 14.5 msec which would put the detonation into tube 2 at 31.2 msec. A 6 msec spark delay was added to prevent backfires, which means the detonation enters the head of tube 2 approximately 37.2 msec after spark.

Instrumentation

Instrumentation varied for each of the tests performed but each setup consisted of a combination of ion probes, pressure transducers, and thermocouples. A pressure transducer was placed in the head of the detonation ignited tube to gather a pressure in the head of tube 2. Ignition time was determined using a RCA (Model 1P28) photo multiplier tube (PMT) shown in Figure 30. The PMT was fitted with a 309 nm high bypass filter to measure light waves emitted by hydroxyl (OH) radicals during combustion. When OH radicals were detected, the PMT outputted a voltage rise indicating ignition had occurred.

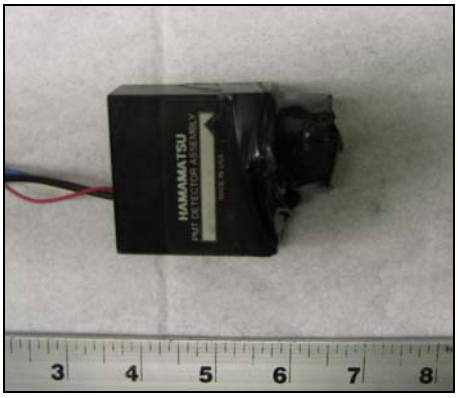

Figure 30. Picture of PMT and filter

The PMT was coupled to a 1 m Ocean Optics multimode fiber optic cable with a 400 micron core diameter and a 24.8 degree acceptance angle the fiber optic cable is attached to an 11.4 cm (4.5 in) fitting, seen in Figure 31, that is mounted in the engine head opposite the pressure transducer.

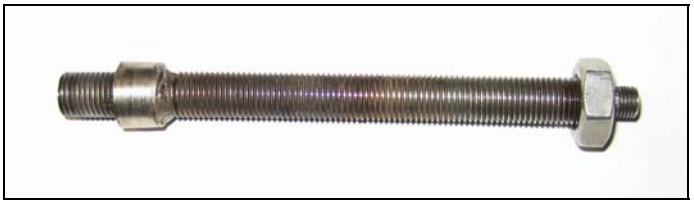

Figure 31. Picture of OH sensor engine head fitting

The PMT is unable to be calibrated to measure OH concentrations because carbon deposits degrade the signal over time. Though the signal amplitude diminishes, the shape of the signal remains intact. The fitting was removed approximately every fifteen minutes of run time to be cleaned. With spark ignition, the concentration of OH radicals mirrors the pressure rise as shown in Figure 32. The data in Figure 32 was run through a high bypass smoothing function (Appendix A) that is displayed for comparison.

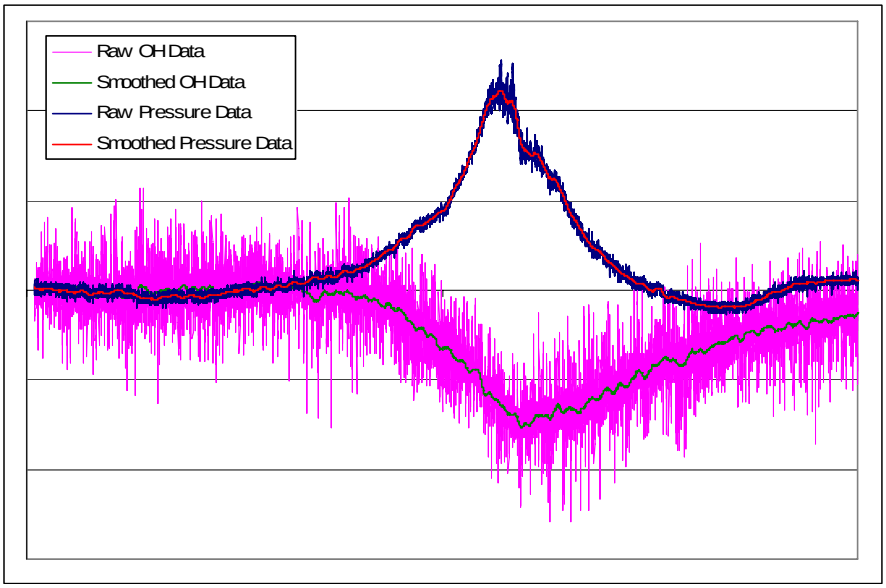

Figure 32. Pressure and OH trace in the head of spark ignited tube

An ion probe is an automotive spark plug used as a capacitor. Five volts is applied to the probe and ions in the combustion wave complete the circuit that discharges the voltage. The drop in voltage is recorded by a LabVIEW program along with the spark, pressure, and OH trace to determine various performance parameters such as ignition time, wave speeds, and DDT time. Figure 33 is a photograph showing the placement of the OH sensor, pressure transducer and ion probes.

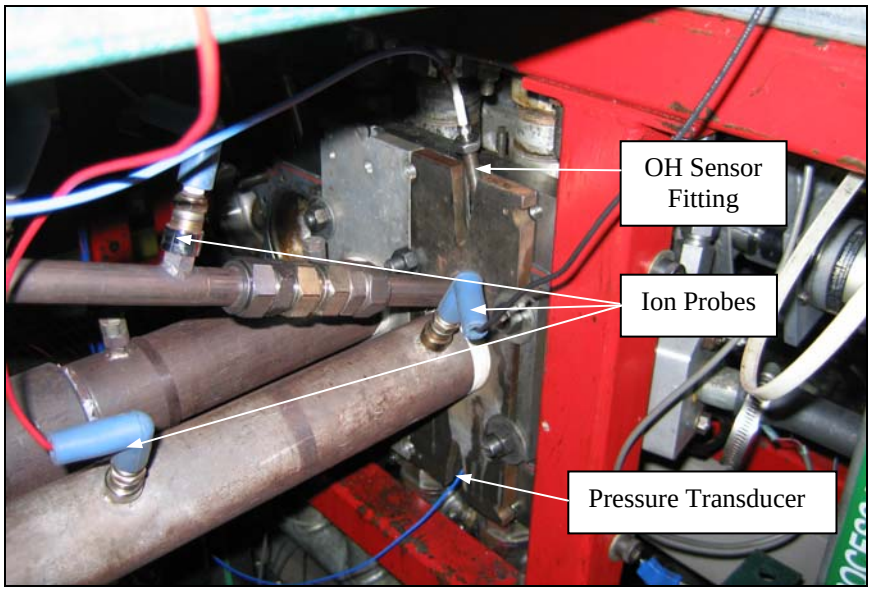

Figure 33. Head of tube 4 with instrumentation

Data Acquisition

The LabVIEW program was set to a master scan rate of 1,000,000 scans per second which captured 500,000 data points for up to 16 individual channels in 0.5 seconds. The output is a binary file containing a continual string of pulse data. At the given scan rate and engine operating frequency, the computer captured approximately eight pulses per data capture. The data files are then read into a separate, in house C++ program called *PT Finder* to perform various performance calculations.

Test Procedures

Before testing the fuel and air mass flow rates were calculated and the corresponding flow number and orifice plates were installed. Transformers were energized and nitrogen bottles were opened to allow control of the test rig. The compressors were actuated and air was blown out of the main air pipes to prevent settled rust and water from damaging the PDE. From the control room, the orifice plates, number of tubes, purge and fill fractions were entered into the low speed computer. The oil pump, water, engine encoder and frequency were actuated by LabVIEW and the main air heater was set to the desired temperature. The desired engine frequency is inputted into the computer and the motor turns the camshaft of the engine. The air, without fuel, is then allowed to flow through the fill and purge lines.

To start the engine, the last chance valve was opened to allow fuel flow and the igniters for both tubes were energized. Tube 2 was also ignited to mitigate unburned fuel being expelled into the atmosphere. The equivalence ratio was then adjusted by increasing or decreasing pressure in the accumulators. The igniter on tube two is turned off once steady state fuel flow and flash vaporization temperatures are reached. Figure 34 is a plot tube temperatures of a typical data collection. The Temperature of tube 4 reached a steady state at approximately 1100 F. The tube 2 temperatures are nearly identical to tube 4 when detonations are present.

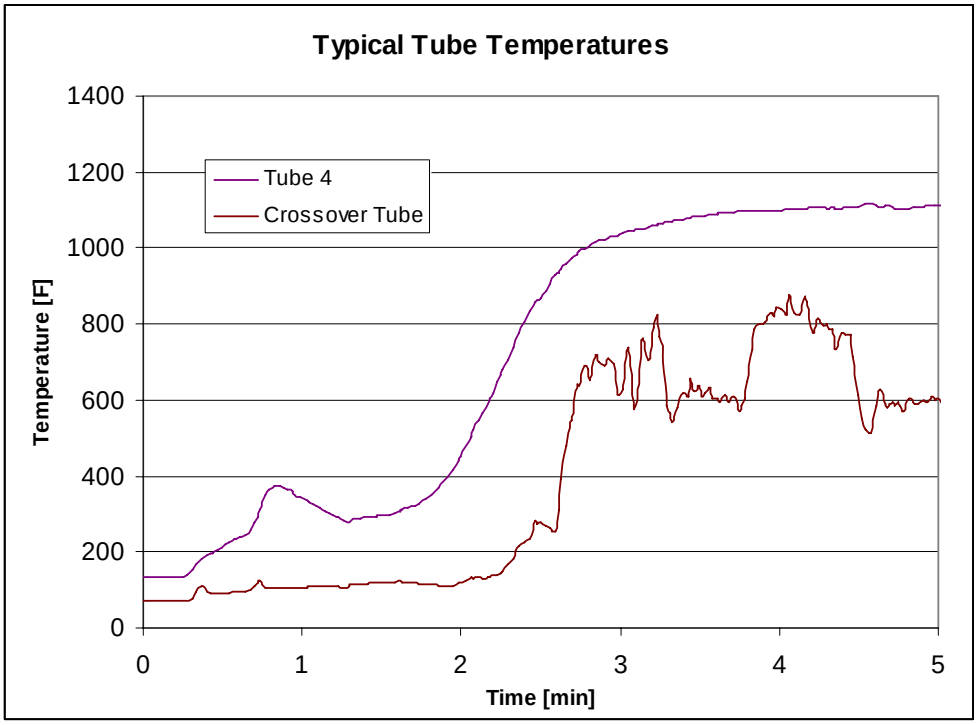

Figure 34. Typical branch detonation tube temperatures

Ion probe data was then gathered by the high speed computer. Upon completion of data collection, the last chance valve was closed and the engine continued to run until the remaining fuel in the line was consumed. The igniter in tube 4 was stopped and the engine was shut down in the reverse order as start up.

IV. Results and Discussion

Due to limitations of the data acquisition system, testing was performed in two phases. The first phase measured wave speeds in the crossover tube and gathered ignition data in the head of tube 2. The second phase involved the instrumentation of tube 2 in order to determine DDT performance. Before continuing, certain terms used throughout the discussion will be defined. Branch detonation is the process of using a detonation from one tube to ignite a second tube. Detonation branching is the process of a detonation from the spark ignited tube entering into a crossover tube. Spark ignition is the process of igniting a detonation tube by a spark plug. Branched ignition is the process of igniting a detonation tube with a deflagration or a detonation wave.

Crossover Tube Instrumentation

Wave speeds in the detonation and crossover tubes were measured by ion probes shown in Figure 35. The measurements shown in the figure are relative to the head of each respective tube. The head of the crossover tube is the portion attached to tube 4.

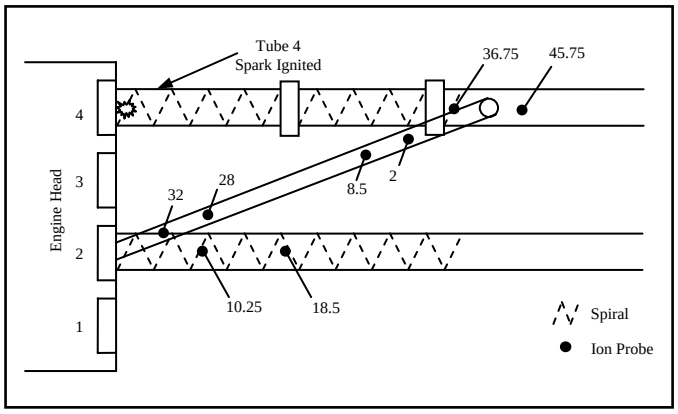

Figure 35. Crossover tube instrumentation

The ion probes in tube 4 measured the wave speed across where the detonation is branched to record the initial detonation velocity. Probes in the crossover tube were used

to create a velocity profile of the combustion front. The probes in tube 2 determine if the detonation wave survives the transition from the crossover to the second tube. For the plots in this chapter, the locations of the calculated wave speeds are assigned a number based on the sequential order of the measured wave speed. For more information on wave speed calculations, refer to Appendix A. The tube numbers are assigned to the corresponding ion probe locations in Table 3.

Table 3. Calculated wave speed locations (Phase I)

Tube Location	Ion Probe Locations [in]	
1	36.75 - 45.75	Tube 4
2	2 - 8.5	Crossover Tube
3	8.5 - 28	
4	28 - 32	
5	10.25 - 18.5	Tube 2

Figure 36 is an example of the type of plots seen in this section. Each data point is representative of the wave speed history of one combustion event. In this case, one combustion event indicates a velocity decrease and the other event indicates a velocity increase through the crossover tube.

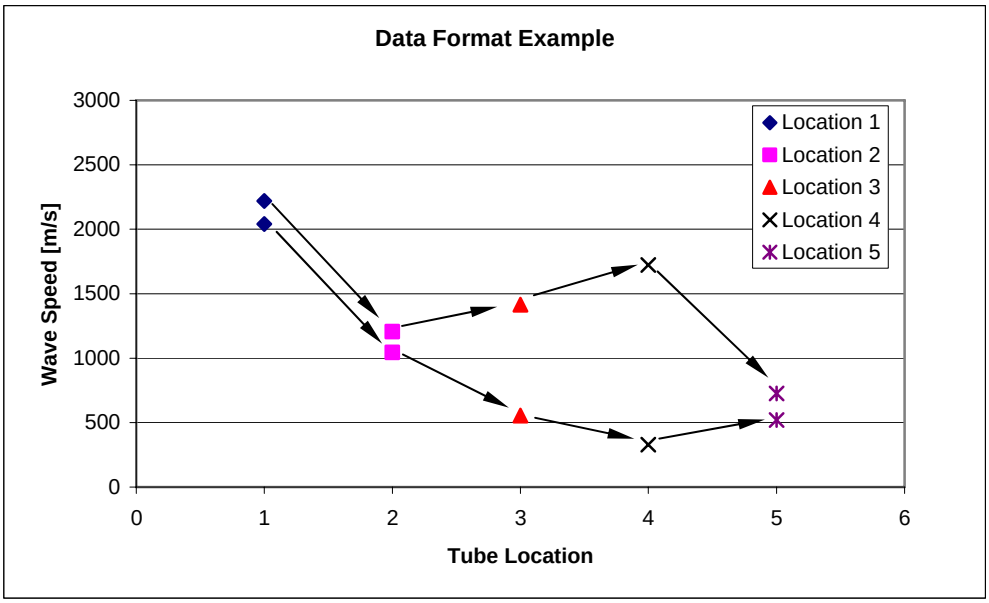

Figure 36. Wave speed data example

Measured Crossover Wave Speeds

The equivalence ratio was varied starting with $\phi = 1.0$, and increased in increments of 0.05. Branch detonation did not occur below $\phi = 1.05$ and failed at $\phi = 1.35$. The first indication of branch detonation was the visible ignition of tube 2 through the closed circuit cameras. Figure 37 indicates the range of wave speeds of combustion events at various equivalence ratios recorded in the first phase of testing.

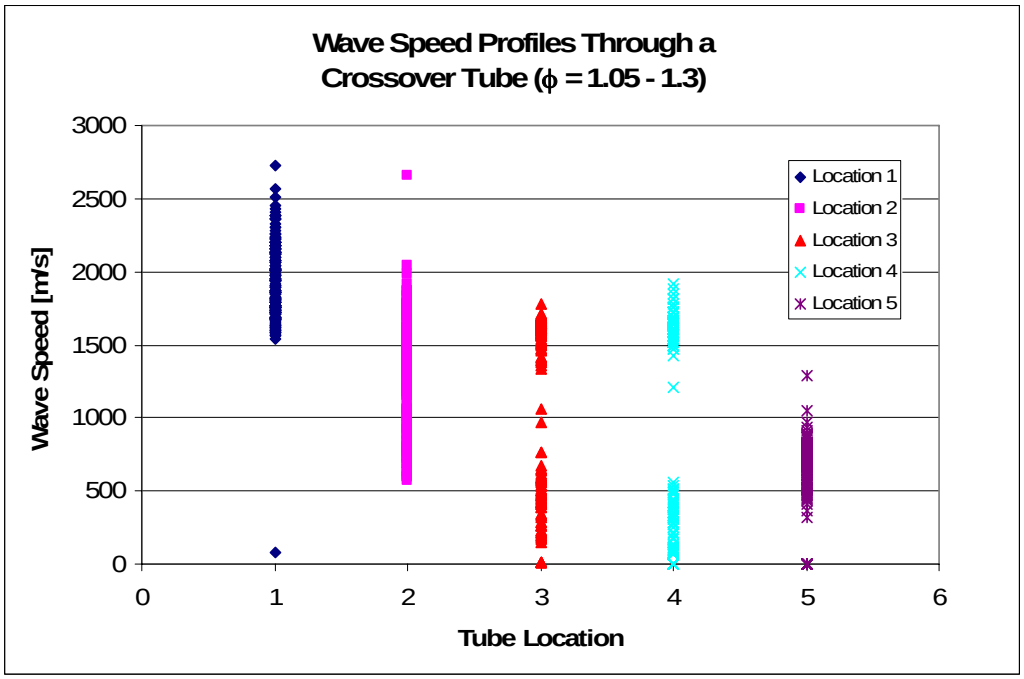

Figure 37. Plot of all data points in the crossover tube

The data scatter at each location is similar regardless of equivalence ratio. Equivalence ratios of 1.2 and 1.25 had fewer instances of wave speeds less than 1400 m/s at location 4, but this will be discussed later. Plots of wave speeds versus tube location are separated by equivalence ratio in Appendix B, Figure 57 through Figure 62. Location 1 in Figure 37 indicates consistent detonations in tube 4, because the wave speeds are all above 1400 m/s. As the detonation branches into the crossover tube, there is a drop in velocity and a large variation in wave speed. The combustion event will either propagate as a

detonation with a wave speed greater than 1400 m/s or decay to a deflagration with a wave speed less than 600 m/s. Wave speeds at location 4 will be used to determine if the combustion event in the crossover tube is a detonation or deflagration, because it is the last measured location before entering the head of tube 2. The wave speeds at location 5 indicate tube 2 was ignited by the branch detonation process, but the detonation decayed to a deflagration as indicated by wave speeds less than 1400 m/s.

Figure 38 is a plot of all wave speeds greater than 1400 m/s measured at location 4. Location 2 indicates a large variation of wave speeds from 1000 to 2500 m/s. As the wave travels down the tube, the variance decreases to wave speeds between 1300 and 1700 m/s. Upon reaching location 4, the wave speeds have increased slightly to a range of 1400 to 1800 m/s. The trend described is the same for all equivalence ratios. The data points in Figure 38 are separated by equivalence ratio in Appendix B, Figure 57 through Figure 62.

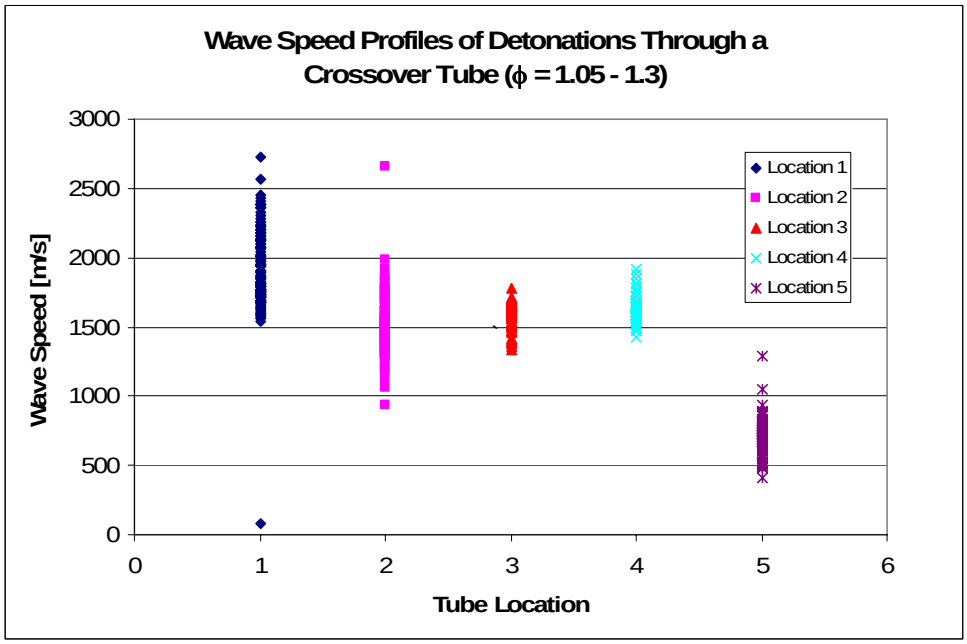

Figure 38. Wave speed profiles of detonations through the crossover tube

The wave speeds at location 3 and 4 are greater than choked flame (wave speeds approximately 1100 m/s) and deflagration speeds, indicating the presence of detonations in the crossover tube. Wave speeds greater than 1400 m/s are considered detonations as is local practice of research performed at D-bay. In house research (Hoke et al., 2005) has indicated the difference in properties (As defined by Table 1 in chapter II) between detonations and choked flames are insignificant. In addition, wave speeds lower than 1800 m/s may be indicative of a single head spin detonation. As stated in chapter II, single head spin detonations have a lower axial velocity and can experience wave speeds less than 10% of the CJ speed. The average wave speed at location 4 is 11% less than the upper CJ value, thus there are indications of a single head spin detonation. Figure 39 is a plot of the average wave speeds at various equivalence ratios of the detonation data points in Figure 38.

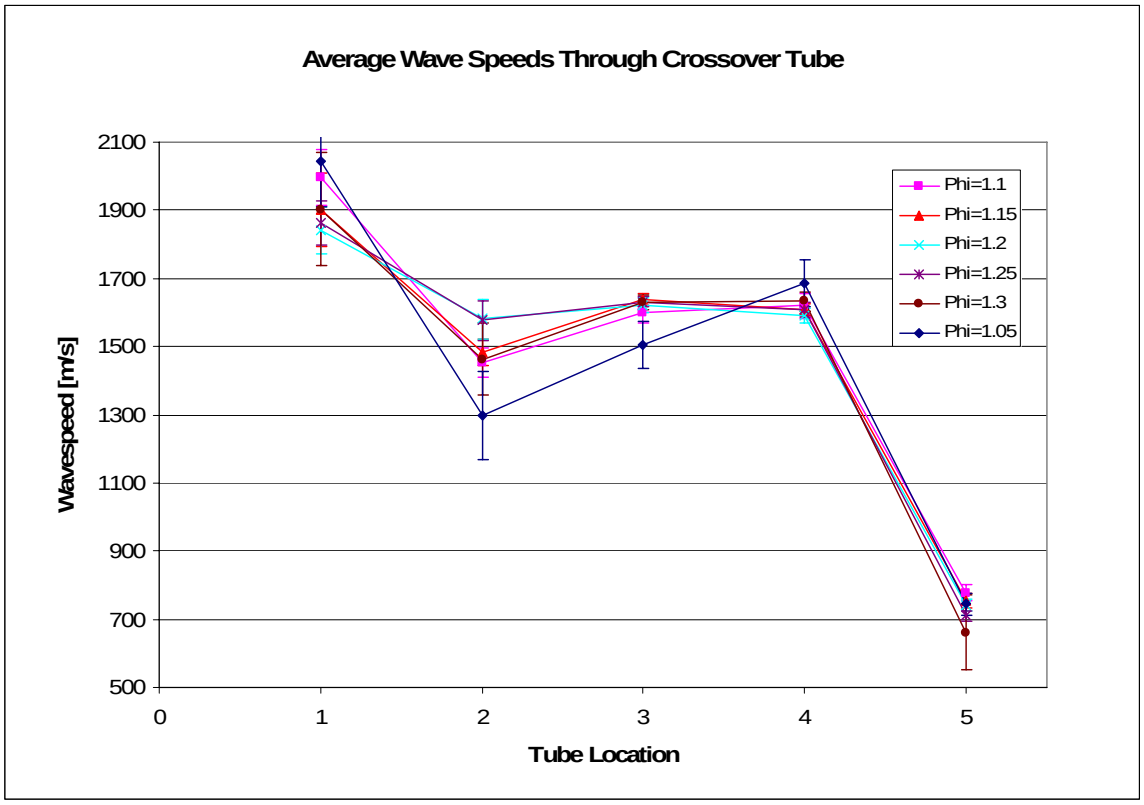

Figure 39. Plot of average speed of detonations through crossover tube

As the combustion front enters the crossover tube, the wave speeds fluctuate at location 2, and then dampen to what appears to be a steady state speed. All equivalence ratios average a velocity of around 1600 m/s at location 4, with a maximum uncertainty of ±100 m/s. The detonation in the crossover tube degrades to a deflagration wave upon entering the tube 2, as indicated by the sharp decrease in wave speed.

Figure 40 is a plot of all wave speeds for which less than 1400 m/s was measured at location 4. The plot shows the branched detonations degrading to in wave speed through the crossover tube, locations 2 through 4. The data points at location 4 are undisputedly deflagrations because the wave speeds are between 5 and 600 m/s. One choked flame was recorded at location 4 and is of no statistical significance. The wave speed then increases as the deflagration propagates into the larger diameter of tube 2, as seen at location 5. The increase in wave speed at location 5 is the deflagration wave beginning the DDT process and will be shown later.

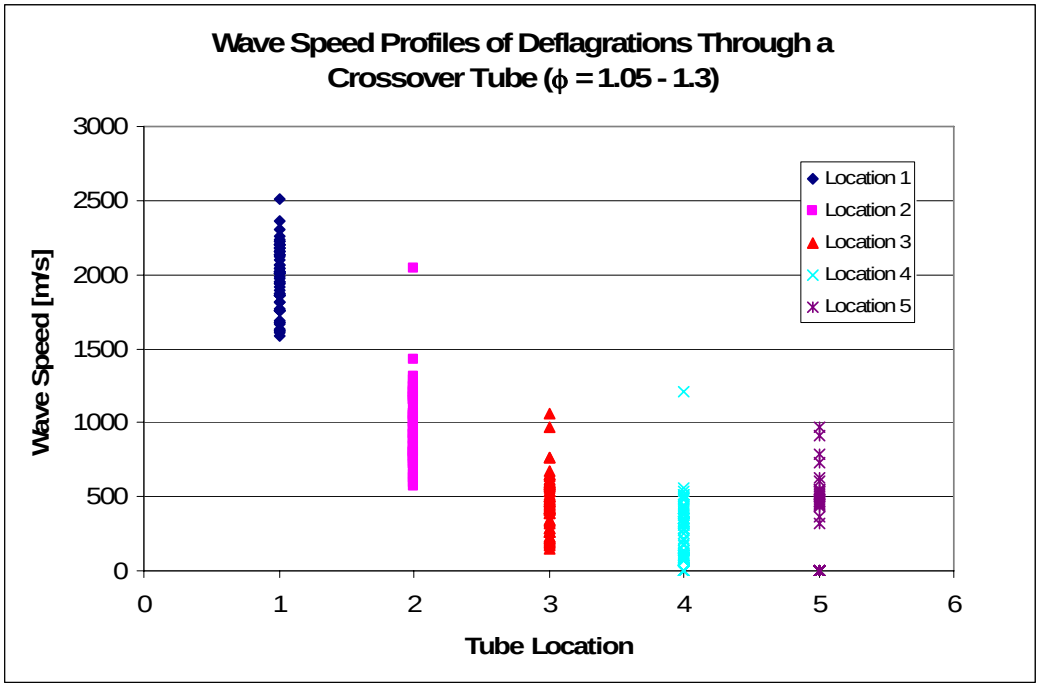

Figure 40. Wave speed profiles of deflagrations through the crossover tube

The likelihood of a detonation propagating through a crossover tube is correlated to the equivalence ratio. Figure 41 shows the percentage of combustion events at location 4 in the crossover tube that are greater than 1400 m/s.

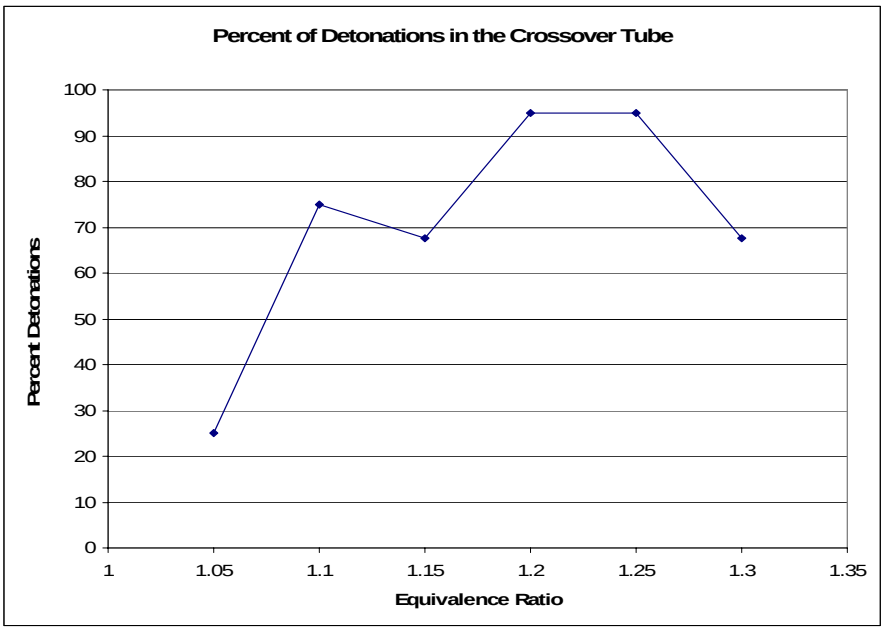

Figure 41. Percent of branch detonations resulting in detonations in crossover tube

The optimum equivalence ratio to propagate a detonation through a crossover tube appears to be between 1.2 and 1.25, as seen in Figure 41. Conversely, the failure mechanism of a detonation wave in a crossover tube is related to equivalence ratio. The low percentage of detonations at $\phi = 1.05$ through $\phi = 1.15$ may suggest that the crossover tube does not have sufficient fuel to sustain a detonation. In addition, boundary layer effects and fictional pipe losses may cause a non-uniform fill of the crossover tube, which could create locally lean areas. The richer fuel-air mixtures may mitigate any lean areas in the crossover tube due to the fill process. On the other hand, a rich mixture degrades the combustion process as indicated by $\phi = 1.3$ in Figure 41. A larger diameter crossover tube would have more fuel to consume and may reduce the amount of deflagrations. An analysis of the fill process of the crossover tube would be beneficial to

determining detonation failure. The performance at $\phi = 1.15$ was unexpected and was not repeated. The data was gathered using the same ambient temperature, pressure and used the same test procedures laid out in chapter III. One would expect the percentage to follow a parabolic shape of the data.

If cell size were a factor in the probability of detonations propagating in a crossover tube, one would expect overdriven waves to produce more detonations. Chapter II stated that overdriven waves can reduce cell size to one tenth of the original. Since the tube size is fixed at ¾ inches, and the critical diameter is proportional to the cell size (based on Equation 16), an overdriven wave appear to be branching into a tube with a diameter much larger than that of the critical diameter; aiding the branch detonation process. Data shows overdriven waves do not increase the percentage of detonations in the crossover tube. Figure 42 is the same data presented in Figure 37, but with detonations less than 1800 m/s at location 1 removed.

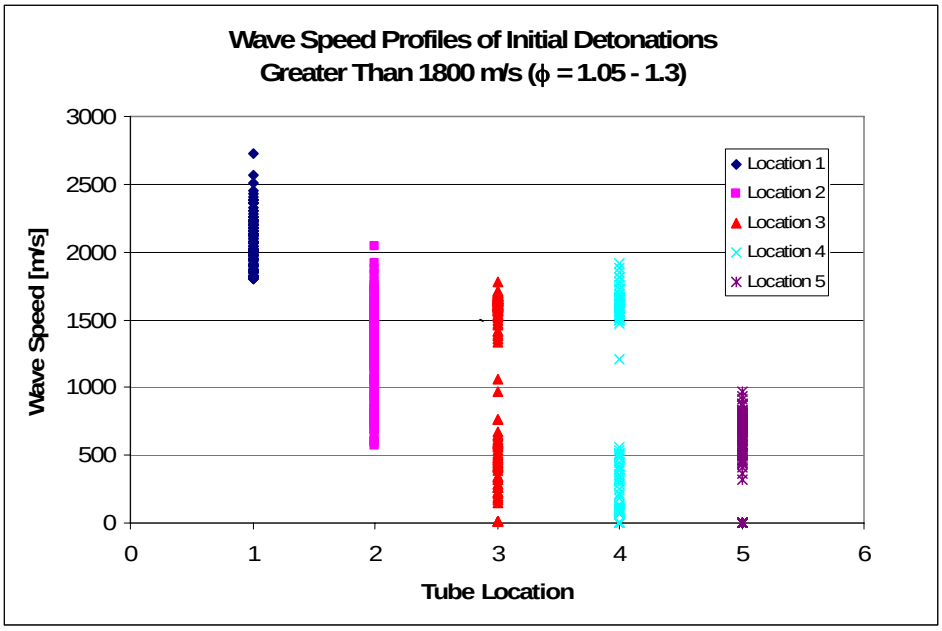

Figure 42. Plot of all data points with initial detonations greater than 1800 m/s

The cell size reduction due to overdriven waves does not affect the likelihood of a branched detonation propagating as a detonation through the crossover tube. Of the data points at location 4, 67% were detonations (wave speeds above 1400 m/s) and 33% were deflagrations (wave speeds less than 1400 m/s) or quenched flames. These wave speed percentages can be compared to Figure 43, which is a plot of all wave speeds with initial detonations less than 1800 m/s at location 1. All wave speeds greater than 1800 m/s have been removed.

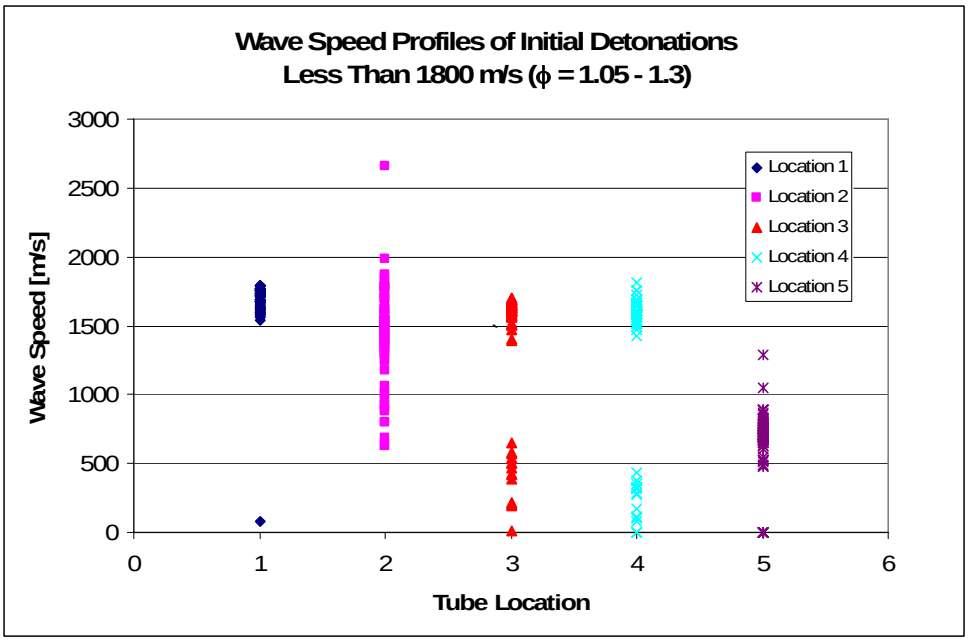

Figure 43. Plot of all data points with initial detonations less than 1800 m/s

Of the data at location 4 in Figure 43, 84% of combustion events were detonations and 16% were deflagrations or quenched flames. The percentage of detonations and deflagrations for Figure 42 and Figure 43 are similar, thus the cell size reduction due to overdriven waves is not correlated to successful detonation propagation through a crossover tube.

Branched Ignition

The PMT and pressure transducer signals were analyzed to determine the ignition time of branched ignition. Figure 44 is a plot representative of pressure and OH signals seen during branched ignition. The pressure and OH trace are plotted as the measured voltage for comparison.

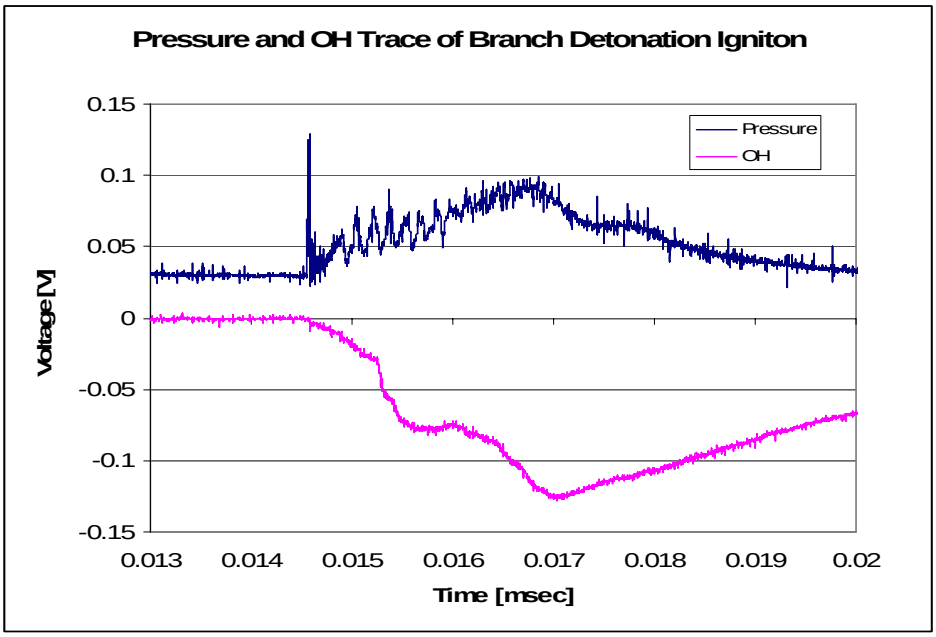

Figure 44. Pressure and OH traces of branch detonation ignition

Figure 44 shows a measured detonation velocity of 1587 m/s at location 4; this indicates a detonation entered the head of tube 2. Previous research using branched detonation, assumed ignition occurred at the pressure peak directly after initial pressure spike (Panzenhagen, 2004). This assumption, however, was incorrect. Figure 44 shows the divergence of the OH trace from the baseline reading (0.0145 msec) at nearly the same instance the pressure increases from its baseline value. The measured OH voltage drop indicates the flame front entered the head of tube 2 and began to consume the fuel. The result is nearly instantaneous ignition of a branched ignited tube. The point of ignition is assumed to be the initial divergence from the baseline value of the OH.

Ignition Performance

The percent of ignitions in tube 2 due to branch detonation is related to equivalence ratio and wave speed. Figure 45 is the percent of all waves, detonations, and deflagrations that result in ignition of tube 2. Once again 1.2 and 1.25 are the optimum equivalence ratios for ignition performance. This is expected since these are the ratios that propagate the most detonations in the crossover tube.

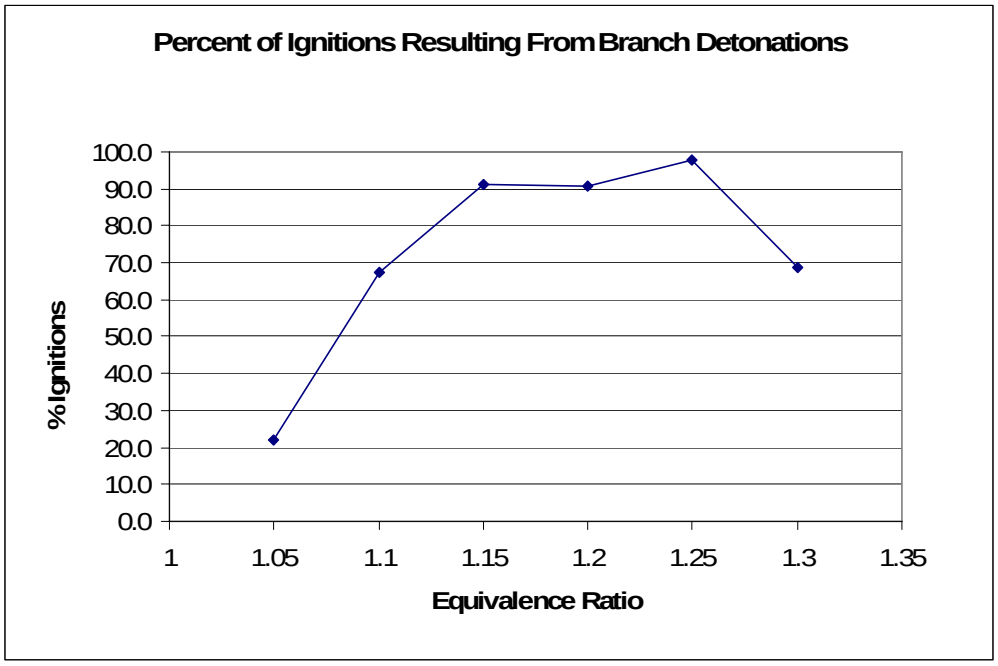

Figure 45. Percent of Crossover detonations resulting in ignition of tube 2

The lean and rich limits such as 1.05 and 1.3, respectively, tend to produce more deflagrations through the crossover tube. Figure 46 is a plot of the percent of ignitions due to detonations exiting the crossover tube, and percent ignitions due to deflagrations exiting the crossover tube. Figure 46 and Figure 41 should be used in conjunction to determine ignition performance. We will evaluate $\phi = 1.1$ as an example.

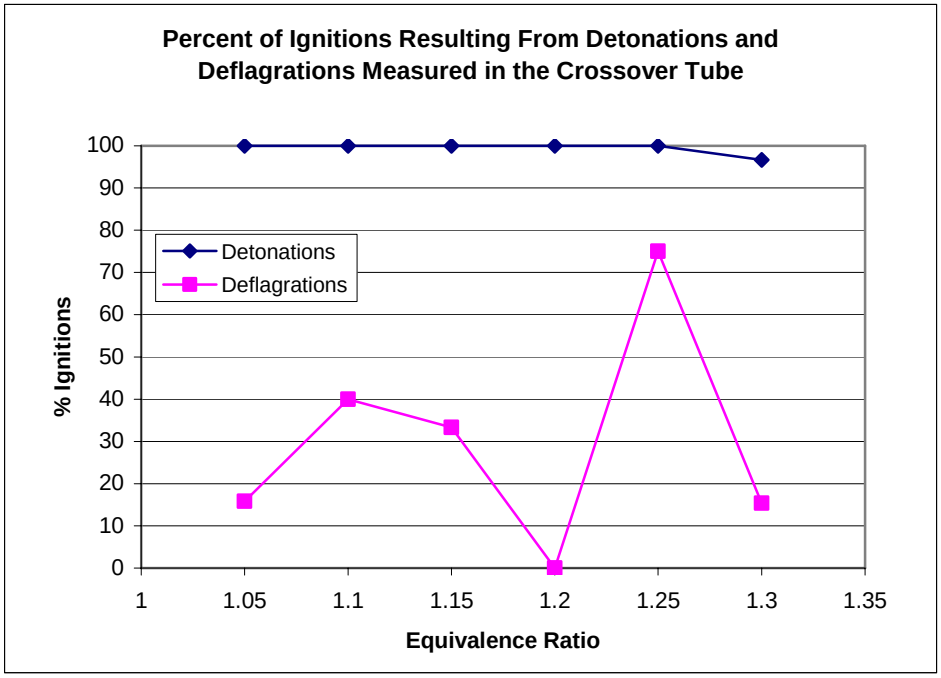

Figure 46. Percent of ignitions resulting from detonations and deflagrations exiting the crossover tube

From Figure 41 at $\phi = 1.1$, we see 75% of measured combustion events were detonations. On the other hand 25% of measured events were deflagrations or quenched flames. Figure 46 indicates 100% of the detonations in the crossover tube at $\phi = 1.1$ resulted in ignition of tube 2. Of the deflagrations measured in the crossover tube, only 40% resulted in ignition of tube 2. The example indicates detonations in the crossover tube are essential for the ignition of tube 2. The percent of deflagrations that ignite the second tube has a much lower performance and does not seem to be dependent upon equivalence ratio.

Spark and Detonation Pressure Comparison

A comparison between spark and branched ignition can be formed by comparing respective ignition times. The definition of ignition time is the time from the deposit of energy to a system, to the formation of a deflagration wave. For spark ignition, the deposit of the spark is the energy into the system, and a pressure rise of 5000 psi/sec is

the formation of a deflagration wave (see Appendix A). Figure 44 has shown ignition time is zero for branch detonation; therefore the initial pressure spike is the energy into the system. Figure 47 is a plot of the pressure trace for branched and spark ignition based upon when energy is deposited into the system.

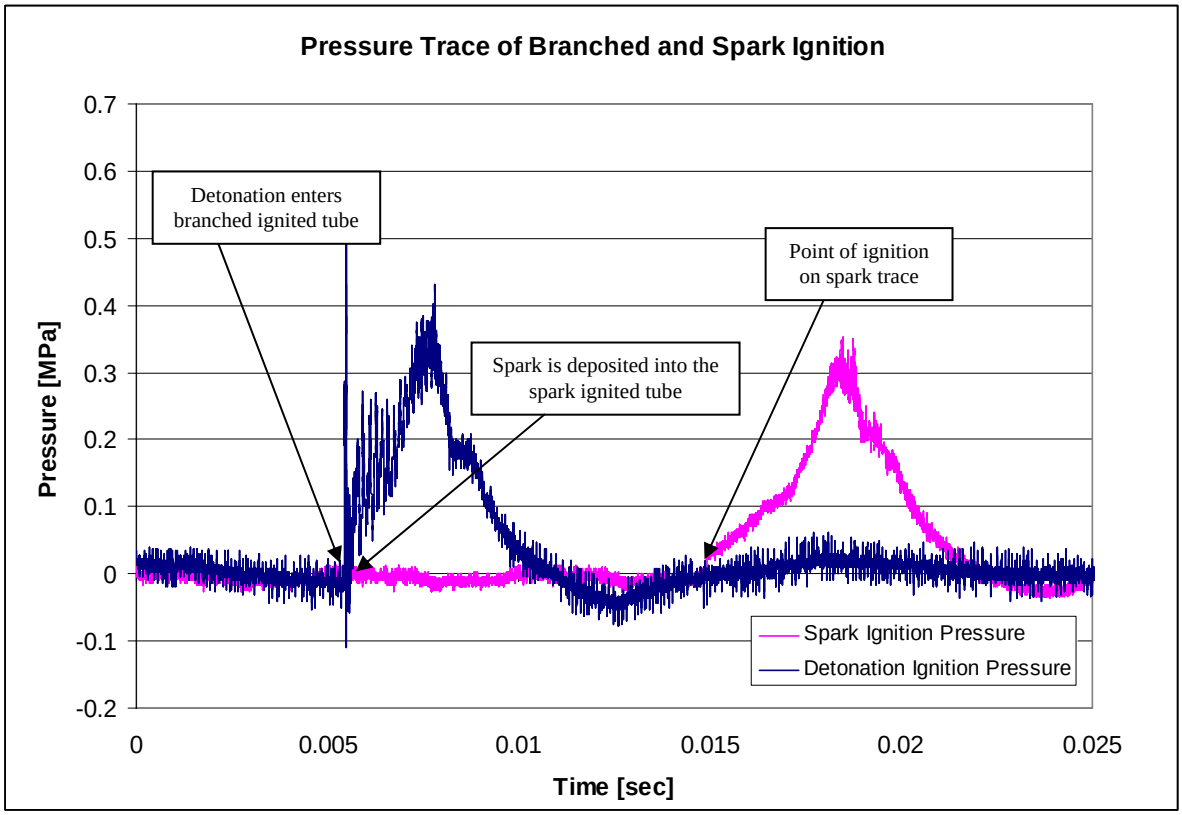

Figure 47. Pressure trace of branched ignition and spark ignition relative to run time

The pressure spike of the branched ignition trace is at the same time a spark has been deposited into the spark ignited system. The branched ignition has reached maximum pressure and exited the tube before ignition has even occurred in the spark tube.

Figure 48 is a comparison of the pressure in a spark ignited and detonation ignited tube normalized to the same ignition time. The branched ignition trace has been shifted to the right until initial pressure spike coincides with the ignition of the spark ignited case.

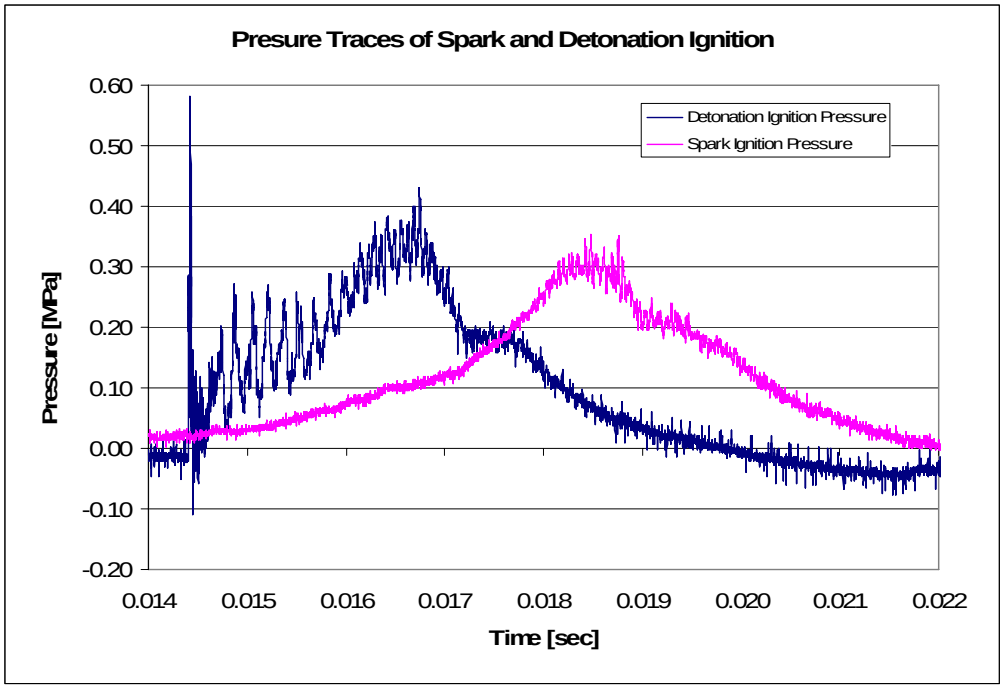

Figure 48. Pressure and OH trace representative of branch detonation

The first difference between the pressure traces is the sharp pressure rise from the baseline value of the detonation. The sharp pressure rise to 0.6 MPa is an indication of the entrance of the detonation wave. If the shock wave of the detonation survived the diffraction process, there would be a step increase in the pressure trace due to the shock wave. There is no step pressure increase in Figure 48, therefore the shock wave has failed. This is another indication the detonation wave did not transition to tube 4. The initial pressure spike is most likely the remnants of the shock wave from a diffracting detonation wave. The pressure traces of spark ignition and detonation ignition are drastically different in time duration. Previous research has shown branch detonation in n-heptane resulted in a larger pressure than the spark ignited case (Panzenhagen, 2004:4-16). This trend is not seen in JP-8 (excluding the initial pressure spike of the branched case), as the maximum pressure of the two traces is almost identical.

DDT Performance

Tube 2 Instrumentation

The second phase of testing was to determine the performance of a branched ignited thrust tube. Performance was characterized by DDT time and location. Ion probes were placed in the crossover and tube 2 as shown in Figure 49.

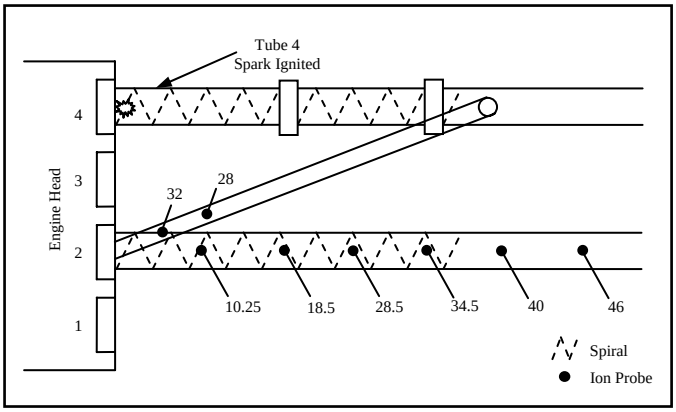

Figure 49. Tube 2 instrumentation

The purpose of the probes in the crossover tube is to measure wave speed of the combustion wave entering tube 2. Ion probes were placed in tube 2 to create a velocity profile of a branch ignited tube. The locations of the calculated wave speeds are assigned a number based on the sequential order the wave speeds are measured. The tube location number continues from the previous section and the cooresponding probe locations from Figure 49 are shown in Table 4. No wave speeds were recorded between the last ion probe in the crossover tube and the first ion probe in tube 2.

Table 4. Calculated wave speed locations (Phase II)

Tube Location	Ion Probe Locations [in]	
4	28 -32	Crossover Tube
5	10.25 – 18.5	Tube 2
6	18.5 – 28.5	
7	28.5 – 34.5	
8	34.5 - 40	
9	40 - 46	

Measured Tube 2 Wave Speeds

Figure 50 is the average wave speed of measured detonations in the system described above. Deflagrations (wave speeds less than 1400 m/s) in the crossover tube were excluded from the wave speed averages at location 4. The measured wave speed versus tube location separated by equivalence ratio is located in Appendix B.

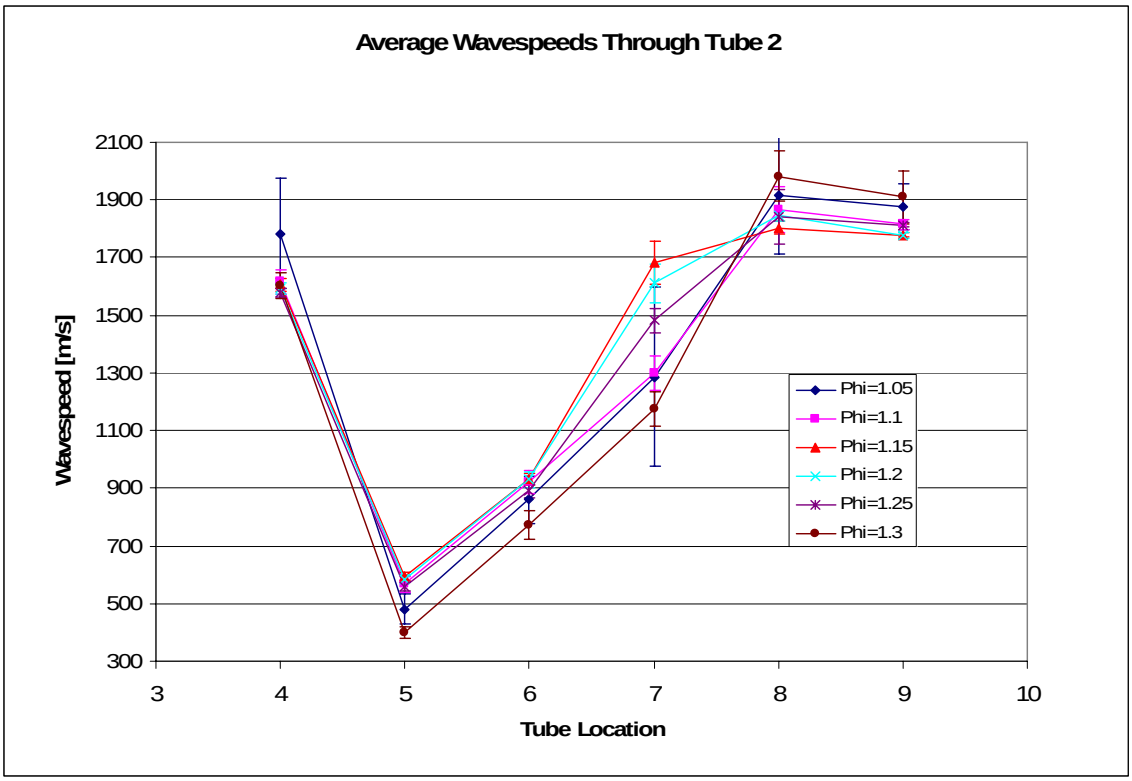

Figure 50. Velocity profile of the detonation transition process

Once again the wave speed in the crossover tube is centered on 1600 m/s. The decrease in location 5 indicates the detonation has failed. Wave speeds at locations 4 and 5 coincide with measurements from the first phase. This demonstrates the repeatability of the system. As the deflagration wave travels down the tube, it is subject to the same DDT process described in chapter II. The wave speeds continue to increase and become overdriven at approximately 0.91 m (36 in), which is the end of the spiral. The wave then settles back to the CJ speed.

DDT Time

Branched ignition reduces DDT time from that of a spark ignited tube. To form a baseline comparison, the crossover tube of the original setup was removed and the crossover ports capped. Tube 2 was spark ignited, and DDT performance was calculated for various detonation wave speed values.

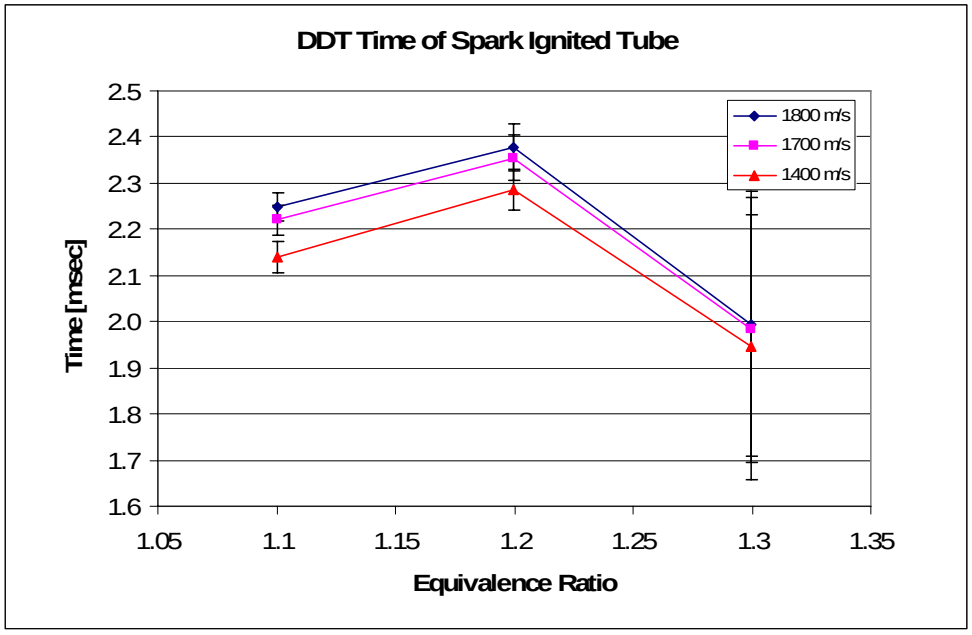

Figure 51. DDT times for various thresholds for a spark ignited tube

Figure 51 shows the average DDT time for 1800 m/s is between 2.2 and 2.4 msec for equivalence ratios of 1.1 and 1.2. An equivalence ratio of 1.3 was too rich for the PDE resulting in sporadic ignitions. Figure 52 is the plot of DDT times at various thresholds for a detonation ignited system.

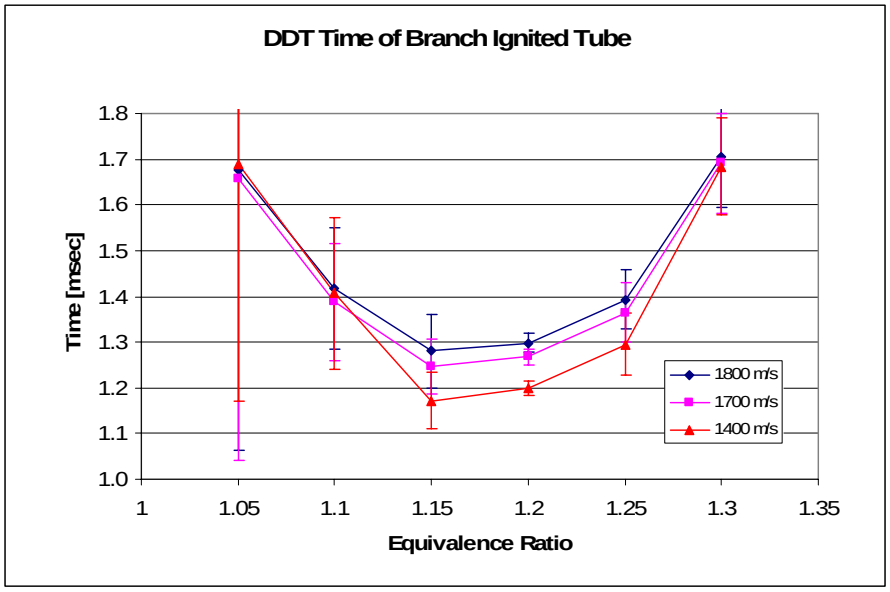

Figure 52. DDT times for various thresholds for a detonation ignited tube

Equivalence ratios of 1.05 and 1.3 are at the limits of branch detonation and produced sporadic detonations resulting in large precision uncertainty. Figure 51 shows an improvement of approximately 1 msec when compared with Figure 51 – a 40% improvement in DDT time.

DDT Location

Unlike branch detonation in n-heptane, (Panzenhagen, 2004:4-22) the location of the DDT did not see a large improvement. Figure 53 is the DDT location of various thresholds for a spark ignited tube.

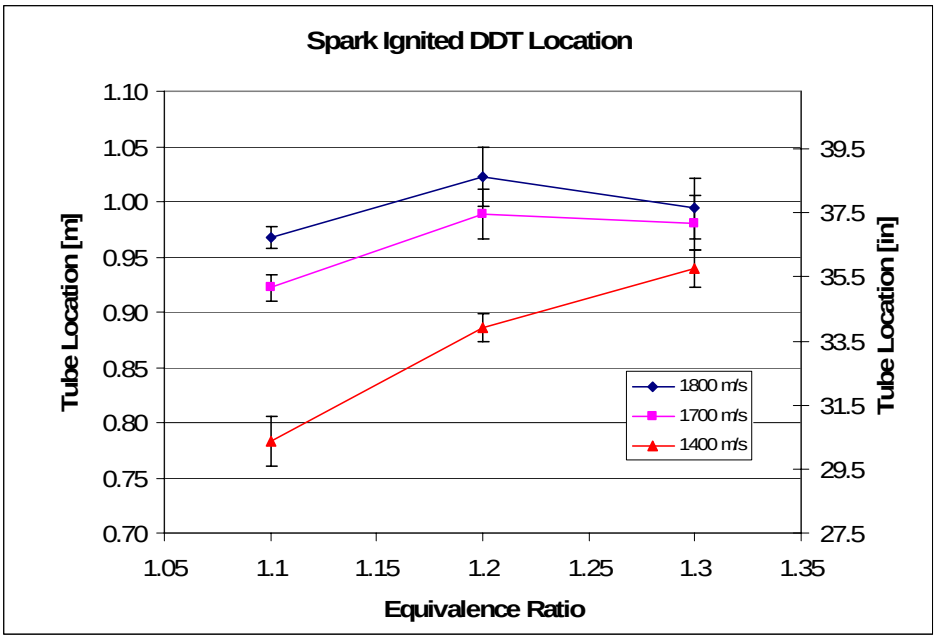

Figure 53. DDT location at various thresholds of spark ignition

Figure 54 is a plot of DDT for the branch ignited case. The branch ignited case has better performance than the spark ignited case. The equivalence ratios experienced little improvement with branched ignition. As indicated by the error bars in Figure 53 and Figure 54, the difference between a spark and branched ignited case fall within the uncertainty of the setup. This indicates no significant savings in DDT location.

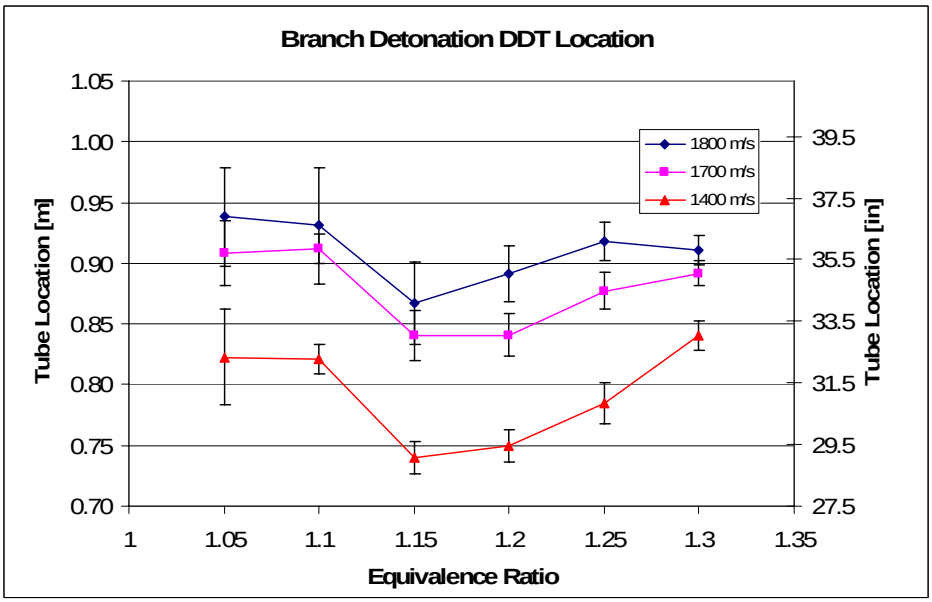

Figure 54. DDT location of various thresholds for detonation ignition

V. Conclusions and Recommendations

Conclusions

This research was the first analysis of branch detonation using flash vaporized JP-8. The counter flow heat exchanger utilized waste heat from the detonation process that allowed steady state data at various equivalence ratios to be gathered. The data showed detonations can propagate in a critical diameter tube, but at a lower velocity than the upper CJ speed of 1800 m/s. In addition, a slightly rich fuel-air mixture of 1.2 to 1.25 had the highest percent of detonations in the crossover tube.

Data showed that branched ignitions are beneficial in decreasing cycle times. By analyzing the pressure and OH concentrations in the head of a branched ignition source, ignition time was shown to be eliminated. In addition to ignition time savings, branched ignition decreased DDT time by 40%. The time savings between ignition and DDT have decreased the fire phase time from 28.5 msec to 2.2 msec. The fill and purge phases can also be reduced to the same order magnitude. The time savings enables valved PDEs to potentially run at operating frequencies between 100 and 150 Hz using liquid hydrocarbon fuels. The increase in operating frequency makes PDEs a viable propulsion source for aircraft and munitions.

Recommendations

PDEs have the potential to run at frequencies higher than 150 Hz if DDT can be eliminated. Continued research should be performed on transitioning branched detonation into a second tube without failure as seen in Appendix C. Doing so would eliminate the use of drag inducing spirals that decrease thrust potential. Shadowgraphs of detonation waves diffracting out of a critical diameter tube and into a larger diameter tube

would give tremendous insight into building a mechanism to transition detonation waves without failure.

Computational fluid dynamic (CFD) models should be improved to model three dimensional effects in a round tube. In addition, the models should be capable of running various chemical kinetics simulations for fuels such as JP-8.

If a self sustaining PDE engine is to become a reality, branched ignition must become more reliable. This research has shown the highest percent of branched ignitions to be approximately 90%, which means a detonation will have to be reinitiated periodically. A sensor could be created that will initiate a spark or a detonation from a separate source, such as a predetonator, to reinitiate the detonation wave. In addition, a timing analysis could be performed on a PDE to determine a method to transition from spark ignition at 35 Hz to branched ignition at 100 Hz.

The setup presented in this report should also be performed with different diameters of crossover tubes. The increase in fuel due to the tube size may provide more energy to the combustion wave and decrease the amount of deflagrations in the crossover tube. In addition, the crossover tube should be analyzed to determine the flow characteristics during the fill phase. A hot wire anemometer could measure velocities and boundary layers of air being pushed through the engine. Doing so may determine why some detonations decay to deflagrations in the crossover tube.

Appendix A: Data Reduction and Error Analysis

Data Reduction

PT Finder

PT Finder converts the binary data into a floating point values. The program then segments each pulse by searching for data between spark signals. The result is an output file containing time stamps and signal magnitudes that can be displayed as in Figure 55.

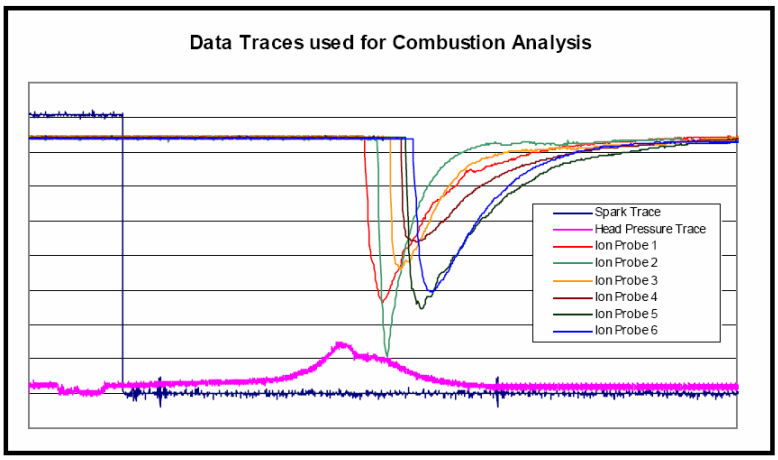

Figure 55. Output of one pulse from PT Finder

Spark Ignition Time

In addition, the pressure trace is sent to a 401 point Savitzky-Golay filter that removes high frequency noise from the signal but retains the shape of the signal. A linear regression is performed on a window of 1000 points. The window moves through the pressure trace a point at a time until a slope of 340 atm/sec (5,000 psi/sec) is detected. The time stamp at the center of the 1000 point window is the time of ignition. Next, the time stamp of the end of the spark is subtracted from the ignition point to determine the ignition time.

Wave Speed Calculations

The program then calculates the time stamp of the point of ion probe discharge. The voltage discharge takes place at the time the combustion wave passes the probe. The program averages the first 500 points to determine the baseline value of the ion probe signal and then looks for the first drop in voltage. With the ion probe time stamps and the distance between ion probes, the wave speeds are calculated and sent to a spreadsheet in units of meters per second. The location of this wave speed is assumed to be in the middle of the two ion probes. *PT Finder* also outputs the time stamps for each of the ion probe discharges that are useful for DDT calculations.

Branched Ignition Calculation

Branched ignition is nearly instantaneous and cannot be determined using the ignition calculator in *PT Finder*. The Savitzky-Golay smoother in PT Finder truncates the pressure signal seen in branch detonation and calculates an incorrect ignition time. A MathCAD program was constructed that ran the OH signal through the same 401 point Savitzky-Golay smoother. Figure 56 shows how the smoothing function truncates the pressure signal of a branched detonation, but accurately resembles the OH signal.

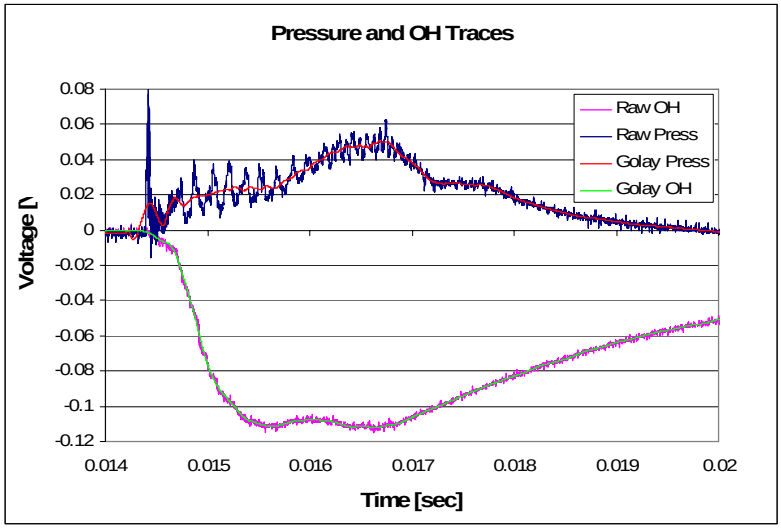

Figure 56. Plot of pressure and OH trace produced by detonation ignition

Once the OH data has been smoothed, the program looks for the first drop in voltage of the smoothed data. The point where the voltage drops is defined as the point of combustion.

DDT Time and Location

A direct interpolation to determine DDT time is not possible since *PT Finder* does not output the time of the calculated wave speed. A MathCAD program was created to mimic *PT Finder* with the exception that it keeps track of the time stamp and tube location of the calculated wave speed. The desired threshold speed, such as the upper CJ speed of 1800 m/s, is inputted into the program. The program searches for the wave speeds above and below the threshold. A simple linear interpolation is performed to calculate the DDT time, and location is then recorded and sent to a spreadsheet.

Error Analysis

The total uncertainty of the system is a combination of bias and precision error. Bias error is the measure of experimental uncertainty due to inaccurate measurements and

data reduction techniques. Precision error is a measure of variation of measurements and calculations. The total uncertainty is determined by Equation (21):

$$U_{\bar{r}} = \sqrt{B_{\bar{r}}^2 + P_{\bar{r}}^2} \tag{21}$$

where $U_{\bar{r}}$ is the *total uncertainty*, $B_{\bar{r}}$ is the *bias*, $P_{\bar{r}}$ is *the precision error*, and *r* is the experimental result of interest (Coleman, 1989:7,94-95).

Precision Error

The precision error is a measure of the variance of the measured events. As seen in chapter IV, many plots display the average wave speed at a location. This average is determined by Equation (22):

$$\bar{x} = \frac{\sum_{i=1}^{n} x_i}{n} \tag{22}$$

where $\bar{x}$ is the *average* of the data, x_i is an *individual data point*, and *n* is the *number of data points in the set* (Milton, 2003:203). The average of a set of data can resemble the approximate trend of the data. On the other hand, there is no measure of precision. This is determined by the standard deviation as shown in Equation (23):

$$\sigma = \sqrt{\frac{\sum_{i=1}^{n} (\bar{x} - x_i)^2}{n-1}} \tag{23}$$

where σ is the *standard deviation* (Milton, 2003:207). The data measured in this research follows a normal distribution that enables the use of another statistical tool known as the confidence interval as shown in Equation (24):

$$CI = \bar{x} \pm \frac{t_{\alpha/2}\sigma}{\sqrt{n}} = \bar{x} \pm P_{\bar{r}} \tag{24}$$

Where *CI* is the *confidence interval*, $t_{\alpha/2}$ is a *T-function* based on the level of confidence required (Milton, 2003:266). The confidence interval is the measure of precision plus or minus from the mean calculated value. The precision calculated for this report is for a 95% confidence interval. This means that 95% of the time, the measured value of the data falls within the confidence interval. The sample size of each tube location at each equivalence ratio is approximately 75 to 100 wave speeds. The precision is shown as error bars on the plots in chapter IV.

Bias Error

Often variables are measured directly and have bias error due to several measurement devices. These are determined by using the root-sum-square equation shown below:

$$B_{\bar{r}} = \sqrt{\sum_{i=1}^{n} B_i^2} \tag{25}$$

Many experimental results are often functions of different measurements that carry their own bias. The building blocks of the desired result are called elemental bias uncertainties. The elemental uncertainties are combined using a root sum square in Equation (26):

$$B_{\bar{r}} = \sqrt{\sum_{i=1}^{n} \left[\left(\frac{\partial r}{\partial X_i} \right)^2 B_i^2 \right]} \tag{26}$$

Where B_r is the *bias of the variable of interest*, r is the *variable of interest*, and B_i is the *bias of each measured variable* (Coleman, 1989:79). Bias errors were calculated based upon the information given below.

Pressure Transducer Uncertainty

The pressure transducers are calibrated within 0.1% of the measured voltage. The maximum voltage is 0.08 V, resulting in an uncertainty calibration of ±0.08 mV. The transducers also have a rise time uncertainty of 1 μsec resulting in ±0.5 μsec. (Helfrich, 2006:72). This effects the spark ignition time calculation.

Air Mass Flow Rate Uncertainty

The air mass flow rate is a function of the pressure transducer, thermocouples, and critical flow nozzles. The pressure transducer is accurate to 0.1% of the full scale value and is ±413.68 Pa. The error of a T-Type thermocouple used is ±3 K. The radius of the critical flow nozzles are accurate to within ±0.0005 in. The result is an uncertainty of ±0.127 lb_m/min.

Fuel Mass Flow Rate Uncertainty

The turbine flow meter was calibrated using a graduated cylinder accurate to 20 mL, resulting in an uncertainty of ±10 mL. A stop watch was used to measure the time to fill the graduated cylinder that was accurate to 0.1 sec resulting in a fuel time uncertainty of ±0.05 sec (Helfrich, 2006:74). Equation (26) was applied to the mass flow rate equation and resulted in an uncertainty of ±0.001 lb_m/min.

Equivalence Ratio

The equivalence ratio is a function of the error in the fuel and air mass flow rates. Equation (26) was applied to the equivalence ratio equation and determined to be ±0.009.

Wave Speed Uncertainty

The wave speed is a function of the distance between the ion probes the time calculations. The ion probes have a response time of 0.1 μsec that results in an uncertainty of ±0.5 μsec. In addition, the ion probe locations were measured to within 1.6 mm (1/16 in) which is an uncertainty of ±0.8 mm (1/32 in). This results in an uncertainty of ±7.53 m/s. The distance between probes is not taken into account in Equation (26). The calculated wave speed is defined to be in the middle of the two probes. In actuality, the wave speed is an average between the probes. In addition, the calculated wave speed could have occurred anywhere between the two probes. This is a downfall of the measurement process, but there are no ways around it. This discrepancy will propagate through for DDT time and location. The distance between the ion probes was not equal, so the maximum distance, 25.4 cm (10 in) in tube 2 will be used for an uncertainty of ±12.7 cm (5 in). This is not desirable, but the larger distance was required to instrument tube 2.

OH Uncertainty

The OH sensor has a response time of 22 nsec. This is very fast and will have little impact on the uncertainty of the ignition time. This uncertainty will also propagate through to DDT time and location.

DDT Time and Location Uncertainty

As stated earlier, the DDT time and location are interpolations between wave speeds, time stamps, and tube locations whose errors propagated through the calculation in accordance to Equation (26). The uncertainty of DDT time is calculated to be ±4 μsec. The uncertainty of DDT location is $\pm 6.7 \times 10^{-3}$ m.

Appendix B: Plots of Wave Speed at Various Equivalence Ratios

Phase I Testing

Figure 57 through Figure 62 are plots of all data recorded in phase I of testing at specific equivalence ratios.

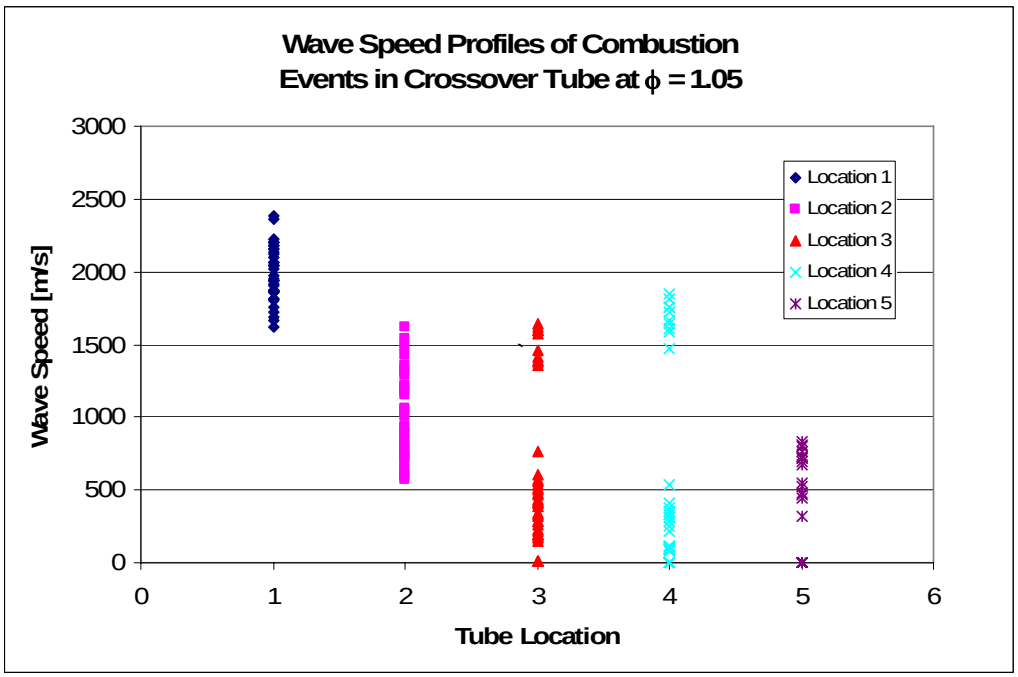

Figure 57. Wave speed data in crossover tube at ϕ=1.05

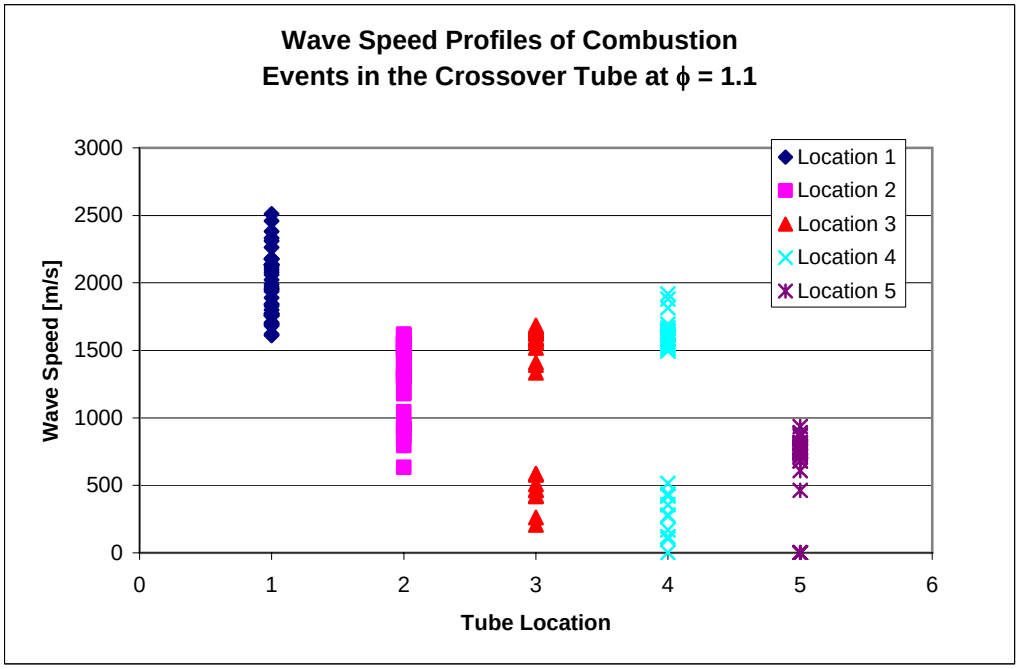

Figure 58. Wave speed data in crossover tube at ϕ=1.1

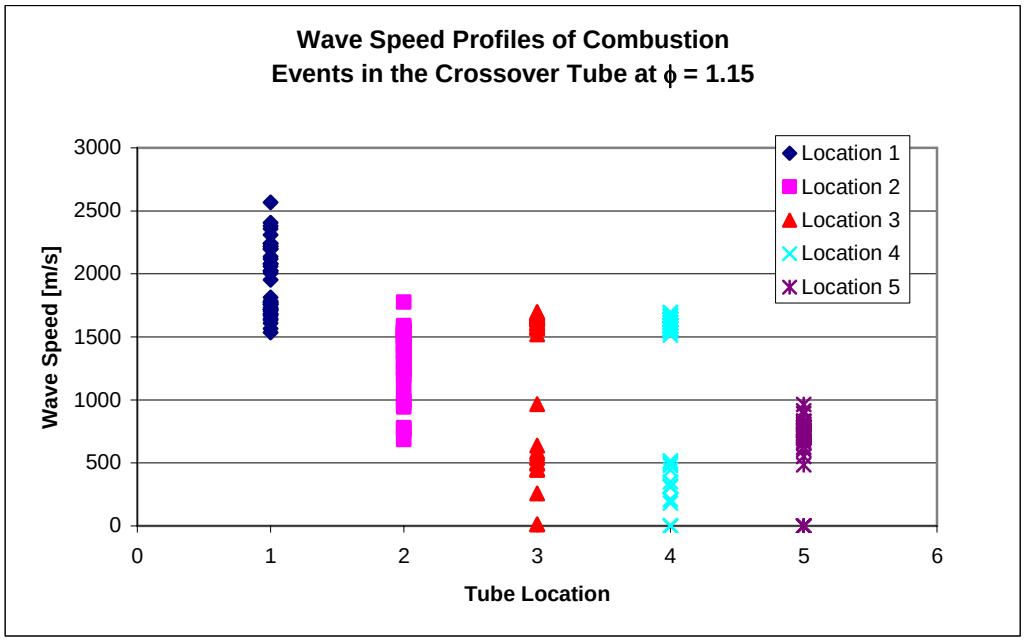

Figure 59. Wave speed data in crossover tube at ϕ=1.15

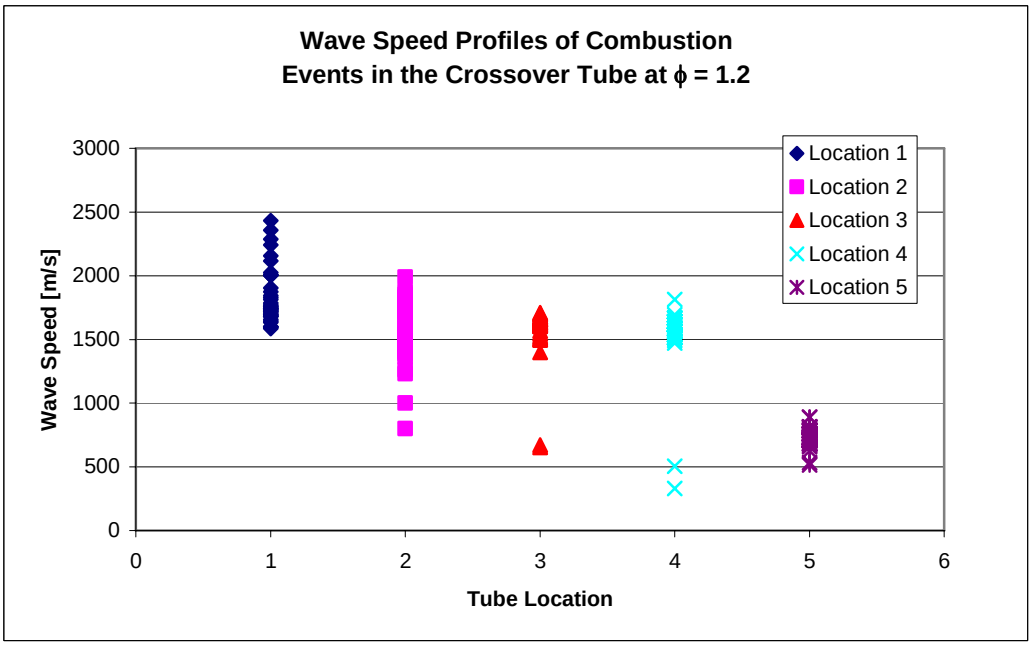

Figure 60. Wave speed data in crossover tube at ϕ=1.2

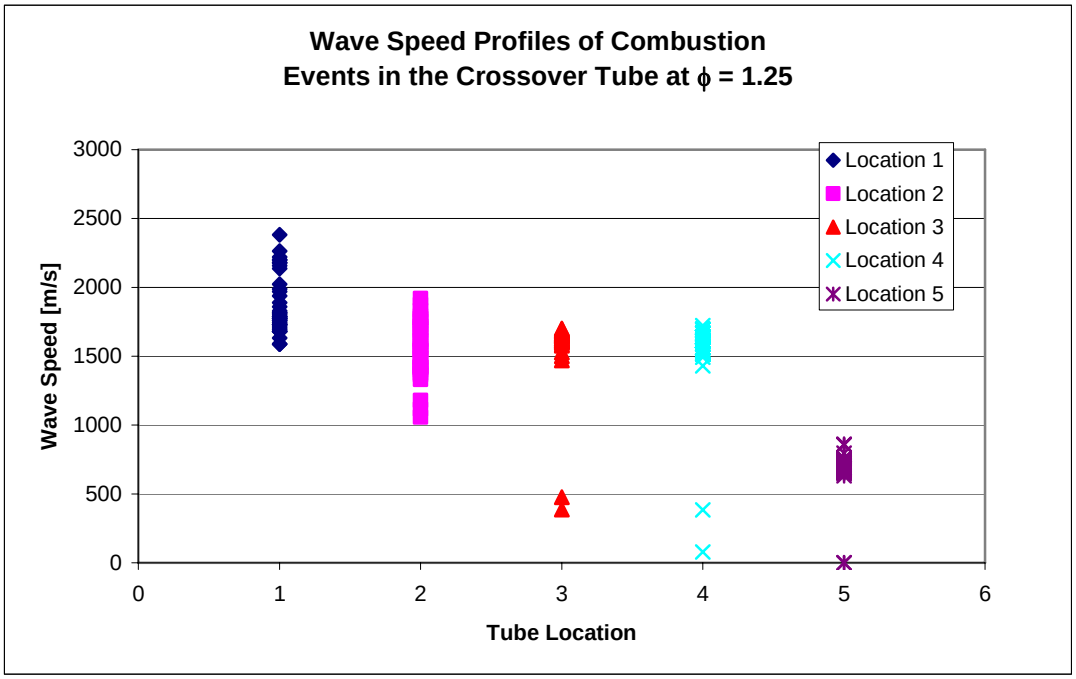

Figure 61. Wave speed data in crossover tube at ϕ=1.25

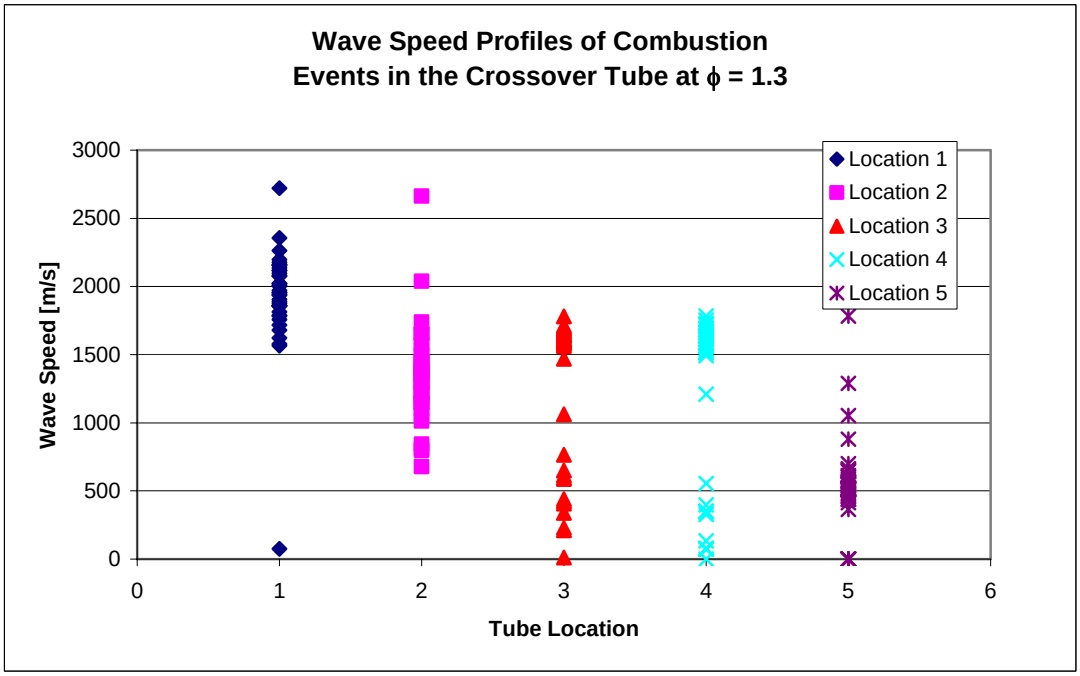

Figure 62. Wave speed data in crossover tube at ϕ=1.3

Phase II Testing

Figure 57 through Figure 62 are plots of all data recorded in phase I of testing at specific equivalence ratios.

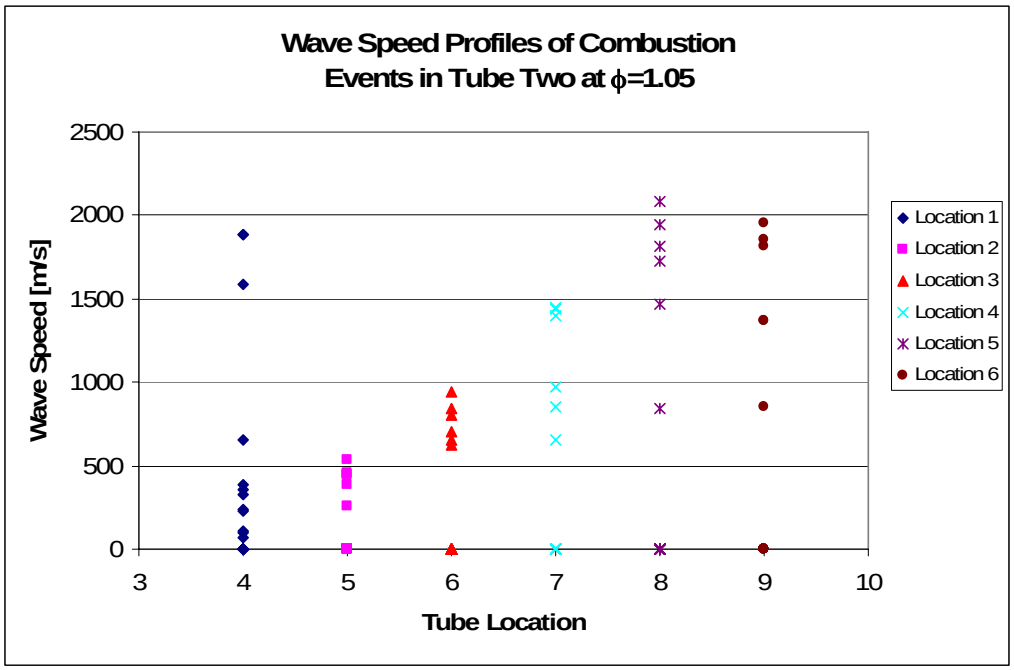

Figure 63. Wave speed data in tube two at ϕ=1.05

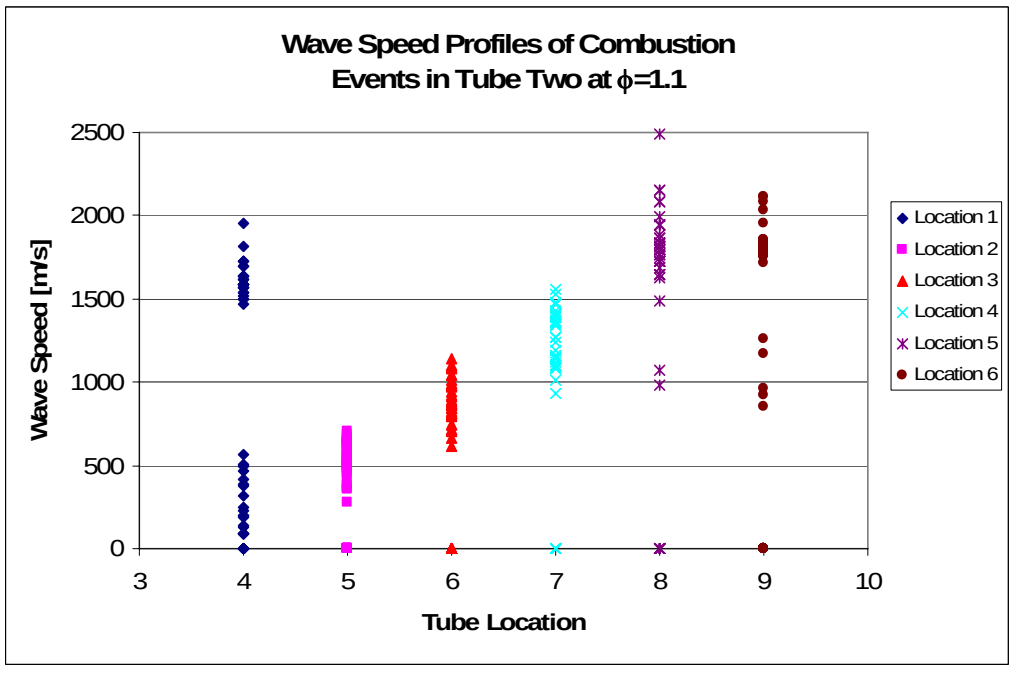

Figure 64. Wave speed data in tube two at ϕ=1.1

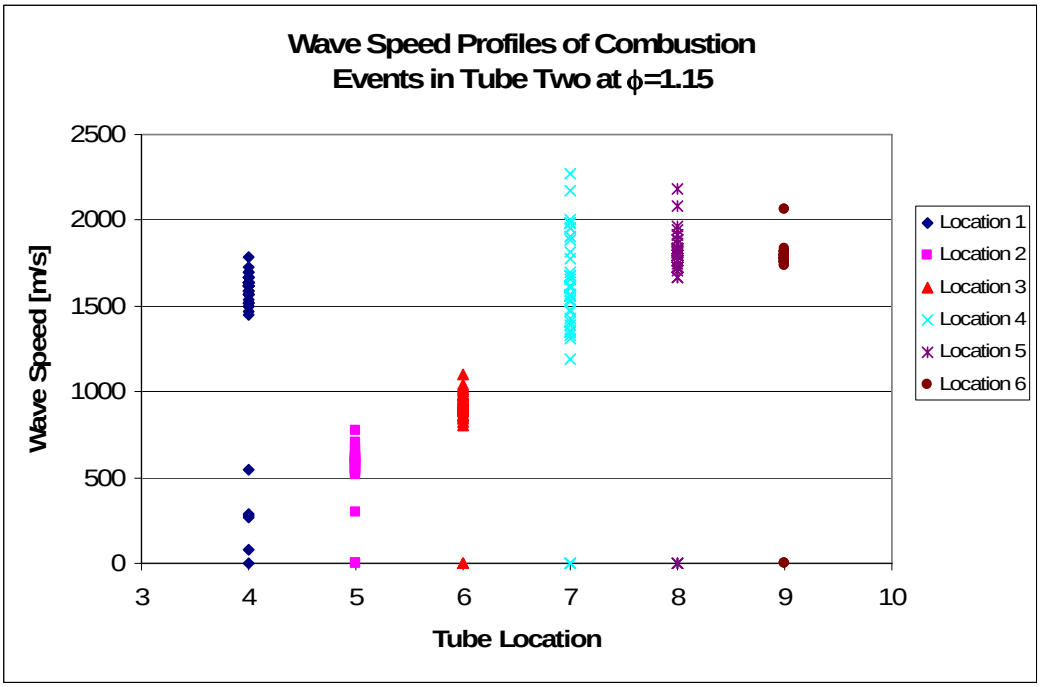

Figure 65. Wave speed data in tube two at ϕ=1.15

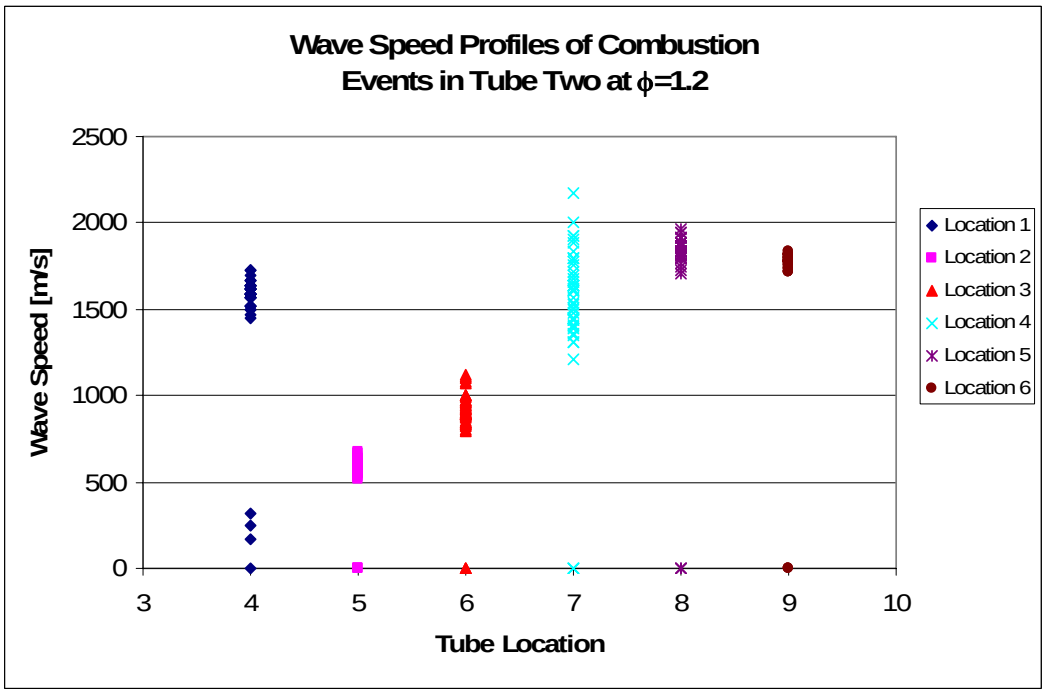

Figure 66. Wave speed data in tube two at ϕ=1.2

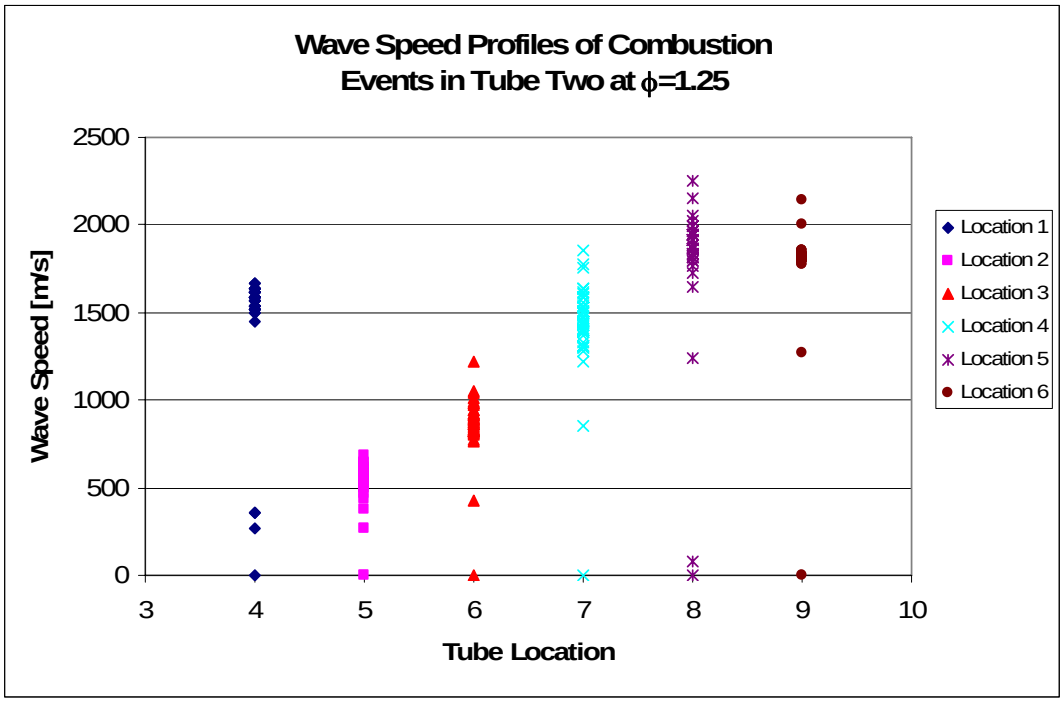

Figure 67. Wave speed data in tube two at ϕ=1.25

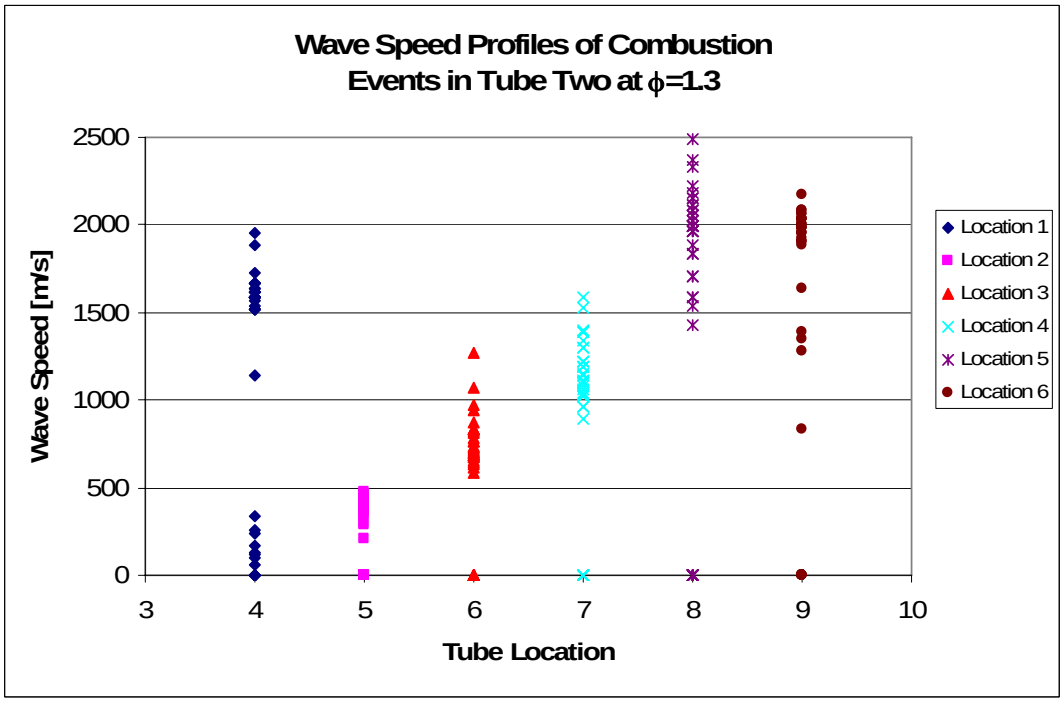

Figure 68. Wave speed data in tube two at ϕ=1.1

Appendix C: Detonation Transition Device

Step Transitions

The idea of diffraction is used in the design of a mechanism to transition a detonation without failure. The research by Schultz (Schultz,2000) shows a diffraction of detonations in the same axial direction. This research attempts to expand a diffracted detonation and direct the path in a direction other than the initial axial pathway. To do so, a series of steps is designed to capture transverse waves and create a somewhat gradual increase in area as seen in Figure 69.

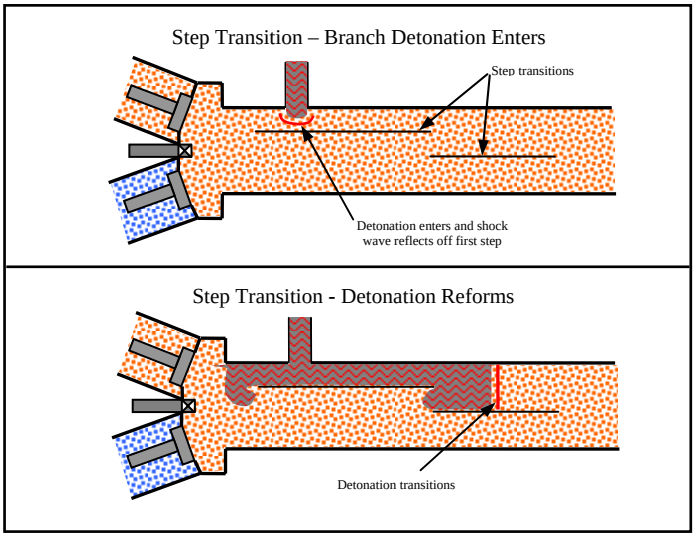

Figure 69. Schematic of step transition concept

Non published, in-house research found steps could perform this task using hydrogen but failed when using avgas. The concept is that the detonation enters the tube and encounters the step transition. The shock wave would begin to reflect off the walls producing transverse waves. The transverse waves would provide the mechanism to reform the detonation wave.

Transition Geometry

The first phase of the testing ported the detonation into the head of tube three, ultimately resulting in detonation failure as discussed in chapter IV. The second round of testing involved the use of transition geometry to attempt to maintain the detonation from the small crossover tube into the larger detonation tube. A housing from the transition geometry was created from a piece of 5 cm (2 in) schedule 40 pipe, 45.7 cm (18 in) in length, with NPT on each end, fitted with a port for branch detonation. The port was a U-shaped tube, 1 in diameter with a 3.8 cm (1 ½ in) diameter bend radius as seen in Figure 70

Figure 70. Photograph of tube three step transition housing

A 1.9 cm (¾ in) U-bend tube was not available; therefore, a male-to-female Swagelock expansion fitting was used to connect the crossover tube to the step transition port. The detonation port was oriented such that the detonation enters tube three pointing slightly upstream. A larger bend radius of the crossover tube to deposit the detonation pointing upstream would have been preferred, but this would have lengthened the crossover tube possibly causing problems filling with fuel-air mixture.

To create the step transitions, a 5 cm (2 in) stainless steel, 0.813 mm (0.032 in) was fitted with a mounting ring similar to the spirals and for the same purpose. The tubing is fitted inside the step transition housing that allows alternate geometries to be interchanged for future research. The steps were constructed by cutting out an arc from 7.6 cm (3 in) stainless steel, 1.62 mm (0.064 in) wall thickness tubing. The 5 cm tubing was cut to form the depths of the steps, and the step pieces were then welded to the 5 cm tubing as seen in Figure 71.

Figure 71. Photographs of step transitions

Step Transition Results

The step transitions above resulted in deflagrations at all equivalence ratios. There was no evidence that detonations were transitioning due to the steps. The failure of the detonations is most likely due to the direction the detonation entered the tube. The next iteration of the step transition should have the detonation entering as parallel to the tube as possible and pointing toward the open end of the tube. Once again, shadowgraphs would aid in understanding the diffraction process. This would allow better understanding in the detonation entrance and step transition design. Angling the entrance of the detonation may transition by taking advantage of the detonation wave produced in super-critical and near-critical detonations.

Bibliography

Coleman, Hugh W. and Steele, W. Glenn, Jr. *Experimentation and Uncertainty Analysis for Engineers*. New York NY: John Wiley and Sons Incorporated, 1989.

Eidelman, S., Grossman, W., and Lottati I. "Review of Propulsion Applications and Numerical Simulations of the Pulse Detonation Engine Concept," *Journal of Propulsion and Power*, Vol. 7:6, (November – December 1991).

Fickett, Wildon and Davis, William C. *Detonation: Theory and Experiment.* New York NY: Dover Publications Incorporated, 1979.

Glassman, Irvin. *Combustion (3rd Edition)*. Sand Diego CA: Academic Press, 1996.

Helfrich, Timothy M. *Cycle Performance of a Pulse Detonation Engine with Supercritical Fuel Injection*. Air Force Institute of Technology (AU), Wright-Patterson AFB OH. March 2006.

Helfrich, Timothy M., King, Paul I., Hoke, John L., and Schauer, Frederick R. "Effect of Supercritical Fuel Injection on the Cycle Performance of a Pulsed Detonation Engine," *42nd AIAA/ASME/SAE/ASEE Joint Propulsion Conference & Exhibit*. Sacramento, CA: AIAA 2006-5133, 9-12 July 2006.

Hoke, John L., Bradley, Royce P., and Schauer, Frederick R. "Impact of DDT Mechanism, Combustion Wavespeed, Temperature, and Charge Quality on Pulse Detonation-Engine Performance," *43rd AIAA Aerospace Sciences Meeting*. Reno NV: AIAA 2005-1342, 10-13 January 2005.

Kuo, Kenneth K. *Principles of Combustion (2nd Edition)*. Hoboken NJ: John Wiley and Sons Incorporated, 2005.

Kaneshige, M. and Shepherd, J.E. *Detonation database*. Technical Report FM97-8, GALCIT, July 1997. See also the electronic hypertext version at http://www.galcit.caltech.edu/detn_db/html/.

Lee J.H., Knystautas R., Chan C.K., *Turbulent flame propagation in obstacle-filled tubes*. Proc Combust Inst 20:1663-1413, 1985.

Milton, J. Susan and Arnold, Jesse C. *Introduction to Probability and Statistics: Principles and Applications for Engineering and the Computing Sciences*. New York NY: McGraw-Hill Higer Education, 2003.

Miser, Christian L. *Pulse Detonation Engine Thrust Tube Heat Exchanger for Flash Vaporization and Supercritical Heating of JP-8*. MS Thesis, AFIT/GAE/ENY/05-M11. Graduate School of Engineering and Management, Air Force Institute of Technology (AU), Wright-Patterson AFB OH. March 2005.

Miser, Christian L., King, Paul I., and Schauer, Frederick R. "PDE Flash Vaporization System for Hydrocarbon Fuel Using Thrust Tube Waste Heat," *41st AIAA/ASME/SAE/ASEE Joint Propulsion Conference and Exhibit,* Tucson AZ: AIAA 2005-3511, 10-13 July 2005.

Panzenhagen, Kristin L. *Detonation Branching in a PDE with Liquid Hydrocarbon Fuel*. MS thesis, AFIT/GAE/ENY/04-M14. Graduate School of Engineering and Management, Air Force Institute of Technology (AU), Wright-Patterson AFB OH. March 2004.

Panzenhagen, Kristen L., King, Paul I., Tucker Kelly C., and Schauer, Frederick R. "Liquid Hydrocarbon Detonation Branching in a Pulse Detonation Engine," *40th AIAA/ASME/ASEE Joint Propulsion Conference and Exhibit*. Fort Lauderdale FL: AIAA 2004-3401, July 2004.

Rolling, August J. *Alternative Pulse Detonation Engine Ignition System Investigation Through Detonation Splitting*. MS thesis, AFIT/GAE/ENY/02-10, Graduate School of Engineering and Management, Air Force Institute of Technology (AU), Wright-Patterson AFB OH. March 2002.

Sarretto, S.R., Lee, S.-Y., Brumberg, C. Conrad, Pal, S., and Santoro, R.J. "Studies of Detonation Transition in a Gradual Area Expansion for multi-cycle PDE applications," *The Combustion Institute,* 2004.

Schultz, Eric. *Detonation Diffraction Through an Abrupt Area Expansion*. Dissertation. California Institute of Technology, Pasadena CA. April 2000.

Schauer, Frederick R, Stutrud, Jeffery, and Bradley Royce P. "Detonation Initiation Studies and Performance Results for Pulse Detonation Engine Applications," 39th AIAA Aerospace Sciences Meeting and Exhibit. Reno NV: AIAA 2001-129, 8 – 11 January 2001.

Tucker, K. Colin. *A Flash Vaporization System for Detonation of Hydrocarbon Fuels in a Pulse Detonation Engine*. Dissertation, AFIT/DS/ENY/05-03. Graduate School of Engineering and Management, Air Force Institute of Technology (AU), Wright-Patterson AFB OH. June 2005.

Tucker, K. Colin, King, Paul I., Schauer, Frederick R., and Hoke, John L. "Branched Detonation in a Multi-Tube PDE," *16th International Symposium on Air Breathing Engines*. Cleveland OH: ISABE 2003-1218, September 2003.

Vita

First Lieutenant John (David) Slack graduated Millard North High School in Omaha, NE in May of 1998. He attended Baylor University in Waco, TX where he graduated with a Bachelor of Science of Mechanical Engineering and a minor in mathematics in 2003. He was commissioned through Detachment 810 Air Force ROTC the same month.

Lieutenant Slack began active duty as an A-10 structures engineer at the Mature and Proven Aircraft Directorate at Hill AFB, UT. A year later he was reassigned as an A-10, T-38, T-37 and QF-4 Aero Performance Engineer. While at Hill AFB, Lieutenant Slack served as an Air Battle Damage Repair (ABDR) engineer. He was qualified on the A-10, F-16, and F-117. In September 2005, he entered the Air Force Institute of Technology Graduate School of Engineering and Management for his Masters of Science in Aeronautical Engineering. His emphasis was in air breathing and rocket propulsion. Upon graduation in December 2006, he will be assigned to the 59th Test and Evaluation Squadron at Nellis AFB, NV as an A-10 flight test engineer.

REPORT DOCUMENTATION PAGE

Form Approved
OMB No. 074-0188

1. REPORT DATE *(DD-MM-YYYY)*	**2. REPORT TYPE**	**3. DATES COVERED** *(From – To)*
20-12-2006	**Master's Thesis**	Sep 05-Dec06

4. TITLE AND SUBTITLE

BRANCH DETONATION OF A PULSE DETONATION ENGINE WITH FLASH VAPORIZED JP-8

5a. CONTRACT NUMBER

5b. GRANT NUMBER

5c. PROGRAM ELEMENT NUMBER

6. AUTHOR(S)

Slack, John D., 1st Lt, USAF

5d. PROJECT NUMBER

5e. TASK NUMBER

5f. WORK UNIT NUMBER

7. PERFORMING ORGANIZATION NAMES(S) AND ADDRESS(S)

Air Force Institute of Technology
Graduate School of Engineering and Management (AFIT/EN)
2950 Hobson Way
WPAFB OH 45433-7765

8. PERFORMING ORGANIZATION REPORT NUMBER

AFIT/GAE/ENY/07-D04

9. SPONSORING/MONITORING AGENCY NAME(S) AND ADDRESS(ES)

AFRL/PRTC
Attn: Dr. Fred Schauer
1790 Loop Road
WPAFB OH 45433-7765

10. SPONSOR/MONITOR'S ACRONYM(S)

11. SPONSOR/MONITOR'S REPORT NUMBER(S)

12. DISTRIBUTION/AVAILABILITY STATEMENT

APPROVED FOR PUBLIC RELEASE; DISTRIBUTION UNLIMITED.

13. SUPPLEMENTARY NOTES

Advisor: Dr. Paul I. King, (937) 255-3636, ext 4628 paul.king@afit.edu

14. ABSTRACT

Pulse Detonation Engines (PDE) operating on liquid hydrocarbon fuels are limited to operating frequencies of 35 Hz due to long ignition times from a low energy ignition sources. This study shows ignition time of JP-8 can be nearly eliminated by igniting a thrust tube using a secondary detonation. A counter flow heat exchanger attached to a thrust tube utilized waste heat from the detonation process to heat JP-8 to supercritical conditions. The fuel flash vaporized when injected into the air stream of the engine. A detonation was produced by a spark in a 5 cm diameter, 1.37 m long tube. The detonation was then propagated in a 1.9 cm diameter crossover tube into the head of second thrust tube where a pressure transducer and hydroxyl (OH) sensor measured the combustion event. Branch detonation was performed over a range of equivalence ratios ranging from 1.05 to 1.3. Branch ignited thrust tubes have shown 40% improvement in deflagration to detonation transition (DDT) time and a slight improvement in DDT distance.

15. SUBJECT TERMS

Pulse detonation engine, branch detonation, detonation ignition, ignition time, deflagration to detonation transition, flash vaporization, JP-8, heat exchanger

16. SECURITY CLASSIFICATION OF:			**17. LIMITATION OF ABSTRACT**	**18. NUMBER OF PAGES**	**19a. NAME OF RESPONSIBLE PERSON**
REPORT	**ABSTRACT**	**c. THIS PAGE**			Dr. Paul I. King
U	**U**	**U**	**UU**	99	**19b. TELEPHONE NUMBER** *(Include area code)* (937) 255-6565, ext 4628; e-mail: paul.king@afit.edu